Gestalt theory for Remote Sensing Image Analysis

Hezron Asukile Mwakisunga
February, 2010

Gestalt Theory for Remote Sensing Image Analysis

by

Hezron Asukile Mwakisunga

Thesis submitted to the International Institute for Geo-information Science and Earth Observation in partial fulfilment of the requirements for the degree of Master of Science in Geo-information Science and Earth Observation, Specialisation: Geoinformatics

Thesis Assessment Board

Chair: Prof. Dr. A. Stein
External Examiner: Dr.Ir. B.G.H. Gorte

Supervisor: Dr. V. A. Tolpekin
Second supervisor: Prof. Dr. A. Stein

INTERNATIONAL INSTITUTE FOR GEO-INFORMATION SCIENCE AND EARTH OBSERVATION
ENSCHEDE, THE NETHERLANDS

Disclaimer

This document describes work undertaken as part of a programme of study at the International Institute for Geo-information Science and Earth Observation. All views and opinions expressed therein remain the sole responsibility of the author, and do not necessarily represent those of the institute.

Abstract

The increased use of Earth observation data acquired by remote sensing technology has enhanced the capability of extracting useful information about the scene being imaged. These data inherently contain information that relates to the type and spatial contents of land cover type. From a general perspective of remote sensing, according to Gestalt principle the human eye relies on visual perception to provide much of the information about the surrounding although it is greatly limited by sensitivity to only the visible part of electromagnetic energy, viewing perspective and inability to form lasting records of what has been seen. From these limitations a continuous development of technological means, increases the ability to see and record the physical properties of the earth in different spectral channels. The techniques for deriving this information from satellite images vary depending on the information required to be observed for proper representation of a phenomenon.

Recently the research has been done on the use of Gestalt principle in extraction of feature from digital images. This principle is the perceptual principle of organization that uses the statistical approach based on phenomenological observations in computing geometric structures in a digital image without any prior information. Based on this principle, many experiments that were conducted by use of grey level photography without tuning parameters performed well for general image analysis. This study concentrates on the implementation of the algorithm based on general principle of perception due to Helmholtz in extraction of linear features from multispectral images.

In implementation of proposed LSD algorithm different parameters such as tolerance of level line angle, image scale and detection threshold epsilon were selected and at different threshold values were tested in order to check the performance of the proposed algorithm based on Gestalt principle to remotely sensed images. The result shows that at the range of 22.5 to 60 degrees for tolerance angle, scale value of 2 and detection threshold value of 0.0 have a greater possibility of obtaining best detection results of multispectral image.

To evaluate the quality of extracted results two approaches (buffer method and visual examination) were used to check the consistence of the meaningful extracted line segment from multispectral image where the extracted dataset was comparing to the reference dataset. By buffer methods where TOP10 vector data was considered as a reference dataset the results show that the dataset containing tolerance angle of 30^{o} equivalent to 6 numbers of orientations, scale value of 2 and detection threshold epsilon of 0.0 gives better results compared to the other datasets tested. Similar results were obtained by visual examination when the objects selected and measure their distances directly from GeoEye image were considered as a true reference dataset.

The results of this study shows that the use of proposed algorithm based on Gestalt principle can also be implemented to multispectral image and give a better results provided that the implementation is done by tuning parameters that control the false detections of line segment in the digital image.

Keywords: Gestalt theory, image analysis, multispectral image, perception, Helmholtz principle, large deviation, gradient orientation, parameter, landsat image, TOP10 vector data and GeoEye image

Acknowledgements

I would like to express my sincere gratitude to The Netherlands Fellowship Program (NFP) and admission Committee of ITC in the year 2008 for offering me the opportunity to study and gain knowledge at ITC, The Netherlands.

Special thanks are addressed to my Supervisors Dr. V.A. Tolpekin and Prof. Dr. A. Stein for their valuable advice, supportive and word of encouragement without tiredness from the preliminary to the concluding level of this thesis, I heartifully thanks because it would have been next to impossible to write and perform this thesis without help and guidance of them.

Great appreciation to Mr. Aiko Mulder, a support officer from ICT Department, who spent his time to install Linux operating system in my machine

I am thankful to Jean Michael Morel, Lionel Moisan and Agne's Desolneux from CMLA, ENS Cachan, France, for their decision to put the Megawave2 scientific software in the public domain. This is a valuable tool to use for researchers in image processing.

My gratitude to my fellow GFM 02, for shared moment especially in academics and social involvement that held at each end of module for the whole study period in Netherlands.

I would also like to thank many other people whom I shared my stay period with here in the Netherlands and for their good company. Special thanks to the student affairs Ms T. B. Van den Boogaard and Ms Marie Chantal for their support during my stay in the Netherlands.

Last but not least, I would like to thank my family, brothers, sisters and my wife Christina for their love, prayers and constant communications.

Table of contents

1. Introduction 9
   1.1. Background 9
   1.2. Problem statement 12
   1.3. Research Identification 13
      1.3.1. Research objectives 13
      1.3.2. Specific research objectives 13
      1.3.3. Research questions 13
   1.4. Innovation aim at 13
   1.5. Outlines of the thesis 13
2. Literature review 14
   2.1. Gestalt theory 14
   2.2. Quantitative Gestalt theory 14
   2.3. Gestalt grouping laws 15
      2.3.1. The law of similarity 15
      2.3.2. The law of proximity 15
      2.3.3. The law of continuity 16
      2.3.4. The law of closure 16
   2.4. Computing partial Gestalt in digital image 17
      2.4.1. Discrete nature of digital image 17
      2.4.1. Gestalt similarity principle 17
   2.5. General detection principle 18
      2.5.1. Detections of alignments 18
      2.5.2. Parameters in digital image processing 19
   2.6. Implementation of Helmholtz principle 19
   2.7. Line segment detection 20
      2.7.1. Megawave2 software 20
      2.7.2. LSD algorithm 20
   2.8. Accuracy assesment 22
   2.9. Related work 22
3. Study area and Data used 24
   3.1. Case study Area 24
   3.2. Data 24
      3.2.1. Image data 24
         3.2.1.1. Landsat7 ETM+ Image 24
         3.2.1.2. GeoEye Image 25
      3.2.2. Topographic map 26
         3.2.2.1. TOP10 vector data 26
4. Methodology 27
   4.1. Geometric transformation 27
   4.2. Detection procedures 27
      4.2.1. A rectangular region 27

4.2.2. Gradient orientation 28
4.3. Line Segment Detection algorithm 29
4.3.1. Subprogram Grad 29
4.3.2. Subprogram RegionGrow 30
4.3.3. Subprogram RectApprox 30
4.3.4. Subprogram ImproveRect 30
4.4. Parameter involved 30
4.4.1. Gradient tolerance angle 30
4.4.2. Scale image parameter 31
4.4.3. Detection threshold epsilon 31
4.5. Strategic feature extraction 31
4.5.1. Parameter selection criteria 31
4.5.2. Feature extraction 31
4.6. Statistical analysis of extracted linear feature 32
4.6.1. Description of the line segment 32
4.6.2. Computing total number of line segment 33
4.6.3. Computing total length of line segment 33
4.7. Concept of validation 34
4.7.1. Pixel coordinate system 34
4.7.2. Mapping coordinate system 34
4.7.3. Points to line conversion 35
4.7.4. Vector transformation 35
4.8. Validation of extracted line segment 36
4.8.1. Matching procedure 36
4.8.1.1. Completeness evaluation 36
4.8.1.2. Correctness evaluation 36
4.8.1.3. Quality assessment 37
4.8.2. Buffer methods 37
4.8.3. Visual examination methods 38
5. Results 40
5.1. Parameter setup 40
5.2. Results based on parameter *d* 41
5.3. Results based on parameter *s* 43
5.4. Results based on parameter *e* 44
5.5. Results of extracted feature 46
5.5.1. Results based on Buffer methods 46
5.5.2. Results based on Visual examination 48
5.6. Summary of the results 51
6. General discussion 52
6.1. Introduction 52
6.2. Performance of LSD algorithm 52
6.2.1. The effect of parameter (d) 52
6.2.2. The effect of parameter s 53
6.2.3. The effect of parameter e 53

6.3. Other comparison methods 54
6.3.1. Gradient orientation base 54
6.3.2. Hough Transform 54
7. Conclusion and Recommendation 55
7.1. Conclusion 55
7.2. Recommendation 56
References 57
Appendices 60
Appendix A: georeferencing result 60
Appendix B: Vector transformation results 61
Appendix C: Statistical results of computations of line segments 62
Appendix D: Computed total reference of line segment and total length of extracted line segment 63

List of figures

Figure 1.1 Remote sensing of Earth resource 9
Figure 1.2: Electromagnetic Spectrum 10
Figure 2.1 Law of similarity 15
Figure 2.2 Law of proximity 15
Figure 2.3 Law of continuity 16
Figure 2.4 Law of closure 16
Figure 2.5 Illustration of Helmholtz principle 18
Figure 2.6 Line segment detected by LSD algorithm 21
Figure 2.7 Undetected mask square in noise image 21
Figure 2.8 Detected square by Gaussian sub-sampling 22
Figure 3.1 Study area 24
Figure 4.1 Regional growing of aligned points 27
Figure 4.2 A line segment 28
Figure 4.3 Search for maximum intensity 28
Figure 4.4 Aligned points along rectangle region 29
Figure 4.5 Approximation of line support region 30
Figure 4.6 left organised vector data and right binary image 32
Figure 4.7 Comparison of extracted and original line segment 33
Figure 4.8 Pixel coordinate system 34
Figure 4.9 Pixel coordinates relation to mapping system 35
Figure 4.10 left matched extracted and right matched reference 36
Figure 4.11 Buffer comparison 37
Figure 4.12 left buffer at 10m and right buffer at 20m 38
Figure 4.13 left buffer at 40m and right buffer at 60m 38
Figure 4.14 Selected objects from Origin Geoeye image 39
Figure 5.1 left origin image and right extracted image at d=4 42
Figure 5.2 extraction at d=6 and right extraction at d=8 42
Figure 5.3 left extraction at d=12 and right extraction at d=16 42
Figure 5.4 left shows average number of lines and right shows the Average length 43
Figure 5.5 left number of lines and right total length when vary d 44
Figure 5.6 left number of lines and right total length against detection threshold 46
Figure 5.7 left Correctness of dataset and right Completeness of dataset 47
Figure 5.8 percentage quality of dataset 48
Figure 6.1 Gradient orientation partitioning 52

List of tables

Table 1.1 Regions for Remote sensing application 10
Table 3.1 landsat image characteristics 25
Table 3.2 Spectral band characteristics 25
Table 3.3 Geoeye image characteristic 25
Table 4.1 Parameter default value 31
Table 4.2 Geo-referenced codes names 35
Table 4.3 Description of the identified feature 39
Table 5.1 Parameter settings 40
Table 5.2 Total number of line segments 41
Table 5.3 Average number of lines and total length 43
Table 5.4 Number of lines and total length at fixed value e=0.0 44
Table 5.5 Trial value for parameter *d* 44
Table 5.6 Number of lines and total length at fixed *s*=2 45
Table 5.7 Completeness of the dataset 46
Table 5.8 Correctness of the dataset 47
Table 5.9 Quality of the dataset 47
Table 5.10 Feature interpretations 48
Table 5.11 Comparison results for land4a2 49
Table 5.12 Comparison results for land6a2 49
Table 5.13 Comparison results for land8a2 50
Table 5.14 Summary of quality measure 51
Table 5.15 Summary for visual interpretation 51

1. Introduction

1.1. Background

Before going on the main concept of this research it is important to start with the remote sensing concept, technical terms like electromagnetic spectrum, energy interaction and sensor characteristics. This will give significant insight on the use of remote sensing image in extraction of useful information about a scene being imaged.

Remote Sensing is the technique of acquiring information about the Earth surface (spatial, area or phenomena) [1], using instruments (sensor) that are designed to record electromagnetic energy reflected or emitted by targeted objects on the surface of the earth without being in contact [2]. Information collected can be in different forms but for the purpose of monitoring and mapping the earth resources the electromagnetic energy distribution for which our sensors that are currently being operated from space-borne or aircraft platforms are used to acquire data [3].

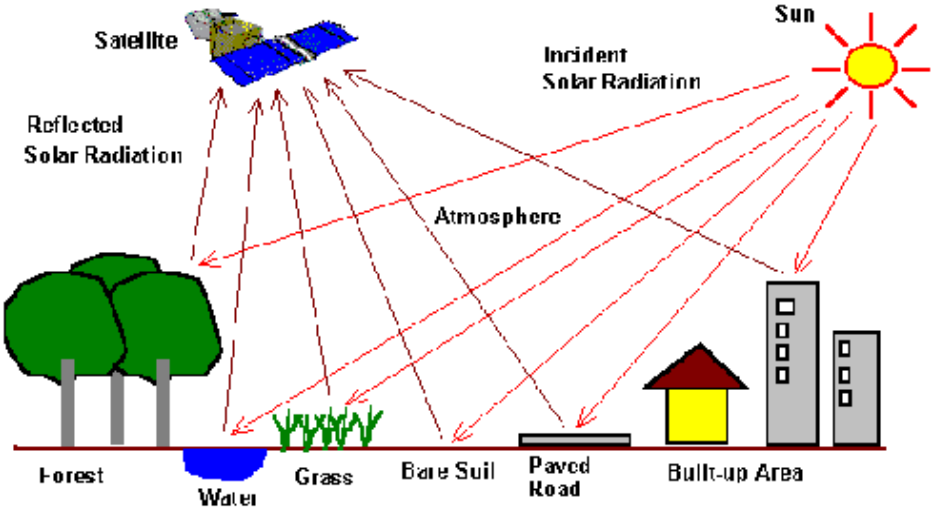

Figure 1.1 Remote sensing of Earth resource (http://rst.gsfc.nasa.gov/Intro/Part2_1.html)

Sensors like Landsat ETM+, GeoEye-2 have a capability of measuring reflected or emitted electromagnetic energy from objects on the earth's surface. The common source of electromagnetic energy is the sun. The energy emitted propagates through and interacts with the atmosphere before and after being reflected from target of interest. Figure 1.1 illustrates the general process of remote sensing [4-5]. The emitted energy is divided into a continuum range of wavelengths known as electromagnetic spectrum. The spectrum ranges from cosmic rays, gamma rays, X-rays to ultraviolet, visible, and infrared radiation, microwave to television and radio waves [5]. The visible part in the electromagnetic spectrum is an important part for human vision and it ranges between 0.4μm and 0.7μm as illustrated in figure 1.2.

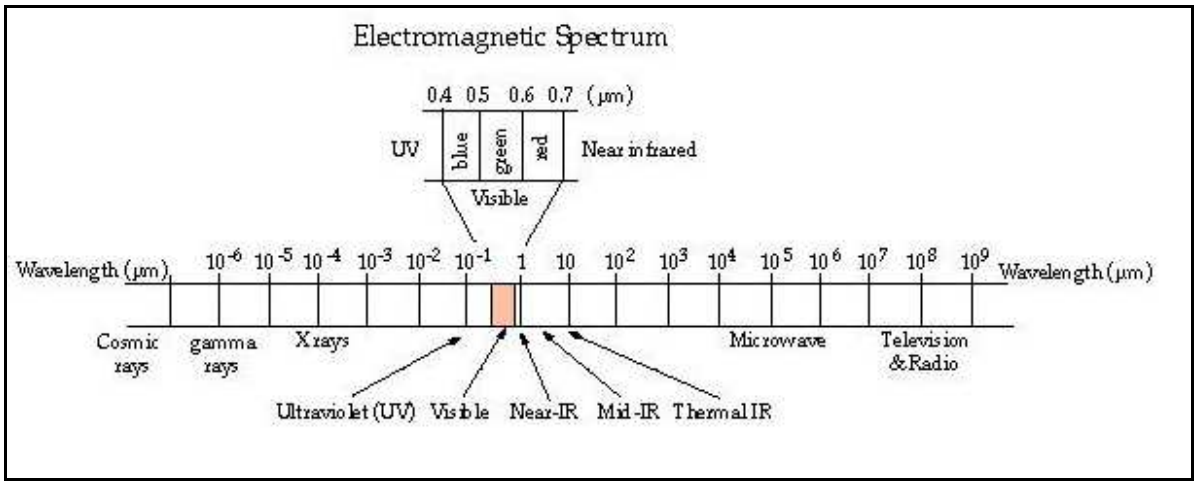

Figure 1.2: Electromagnetic Spectrum
(http://www.ucalgary.ca/UofC/faculties/SS/GEOG/Virtual/Remote%20Sensing/spectrum.gif)

Band selection for visual interpretation and classification is an interesting task in remote sensing which requires studying the spectral sensitivity of the sensor available to detect and record the energy reflected by objects. The interaction and the interdependence between the primary sources of Electro-magnetic energy, the atmospheric windows through which source energy may be transmitted to and from the Earth's surface features is an important elements to consider when selecting bands[3]. Table 1.1 shows the further subdivision of an important region for remote sensing applications.

Name	**Wavelength (μ m)**
Optical wavelength	0.30-15.0
Reflective 1. Portion Visible 2. Near IR 3. Middle IR	0.38-3.00 0.38-0.72 0.72-1.30 1.30-3.00
Far IR (Thermal, Emissive)	7.00-15.0

Table 1.1 Regions for Remote sensing application

The human eye is sensitive to light and it attains its peak sensitivity at 0.55μ m in the green part of the visible Spectrum [6]. From a general perspective of remote sensing according to Gestalt principle, human eye relies on visual perception to provide with much of the information about surrounding compared to computer vision although it is greatly limited by sensitivity to only the visible part of electromagnetic energy, viewing perspective and inability to form lasting records of what have been seen. From these limitations a technological means are continuously increased and the ability to collect different images at once and record the physical properties of the earth in different spectral channels is now possible. Different techniques for deriving this information from satellite images are researched and vary depending on the information required to be observed for proper representation of phenomenon.

Visual recognition of an object or pattern in images according to Gestalt psychology is an effect to the form forming capability of sensation. Human eye has a greater capability of interpreting object or pattern in the image better compared to computer vision[7]. In order to extract information from the

image, different techniques such as digital image analysis and image enhancement are performed. In the field of computer vision, feature extraction plays an important role on the performance of scenes analysis.

Image analysis has become an essential part in extraction of useful information used as an input in geographical information systems(GIS) and for spatial decision making [8]. Previously the image resolution was a limiting factor on interpreting and extracting objects or patterns in image. The improvement of the instrument used to collect a lot of information about the earth resources has provide a fully benefit of using computer to extract automatically useful information that are impracticable to do it manually. The knowledge of using computer in extraction of information from digital images results in the increase of the number of theories and algorithms. This rapid increase aimed at predicting all basic perception associated with digital images being fully automatically extracted and significantly contribute to improve the efficiency of extraction of features in the images[9].

Data mining refers to the process of extraction and analyzing data from different perspectives and summarizing it into useful information [8]. In remote sensing the data collected using sophisticated instruments becomes one of the sources of information for various applications. Extraction of information to a large volume aims at reducing uncertainty for making better decisions [10]. In this case intelligent procedures to deal with various characteristics of image data are required for the purpose of obtaining meaningful information. In practice, remote sensing technology uses a variety of devices for gathering information that are used to construct the image at different resolution. This image resolution is the measure of the amount of details the image holds.

A significant advance in sensor technology stemmed from subdividing spectral ranges of radiation into band allowing sensors that produce several bands of differing wavelengths to form multispectral images [11]. Multispectral imaging can allow extraction of additional information that the single band image may fail to capture but for its possibility to have more than three bands it can restore information.
For better interpretation of multispectral image data the first stage that is performed includes the rectification and restoration of acquired images [3]. This initial processing of raw image data eliminates geometric distortion and reduces the presence of noise in the image [12]. Most of preprocessing of remote sensing image is done by the distributers but the geometric transformation for geometric integrity of the map for better evaluation may be done by the users.

Gestalt theory was the outcome of research in psychology between 1923 and 1975. The theory is based on the knowledge of the laws of perceptual organization and emphasizes on how to group and construct an object or feature from the image [9]. Recently several researches used single band (gray level) images for image analysis based on gestalt principles and yield better results. The use of Gestalt principle to multispectral images in analyzing remote sensing images has not been researched in the area of growing research and this motivates the research to apply the Gestalt principles for remote sensing images in the detection of the geometric structures such as linear feature etc.

Gestalt is a German word translated as a whole, form or configuration that recognizable has parts which can be experienced as an indivisible unity. The basic elementary Gestalt grouping laws

includes proximity, similarity, closure, continuity and simplicity which are also called the laws of perceptual organization and can be explained in the context of perception and problem-solving[9]. In quantitative Gestalt these grouping laws have a mathematical interpretation and can combine together to form larger object called global Gestalt [9]. In remote sensing the algorithms applied to grouping laws can also give a better result to digital remote sensing images. For example the Gestalt law of good continuation and determination of meaningful contrasted boundary in remote sensing image analysis relate to the pixel based classification where by similar pixels with the same spectral value are grouped together. The law of similarity can be used in determine the number of classes in the images during preprocessing by study of histogram where meaningful gaps and peak are defined.

A major function of perceptual organization is to distinguish non-accidental groupings from the background of groupings that arise through accidental in the identically distributed random noise [9]. According to Helmholtz principle any structure or entity in the white noise can only be perceived if there is a large deviation from randomness. From this principle Desolneux provided a general mathematical principle that does not use any a prior or learned model but make use of a contrario model which based on local independent assumption [9]. In this model two regions are meaningfully different if the probability of observing such a different is very low in the pure noise. Suppose if l is the length of line to be detected and k is the number of points assumed to be aligned in the line at a precision p in an image of size N then the detection can be expressed as a threshold function of the number of false alarm given by

$NFA_{k\min} \geq (l, p, N)$ for any alignment to be detected in the white noise image

Where; k min is the threshold function at minimum

l is the total length of an alignment

p is the precision of alignment

N is the size of image

When computing detection thresholds it is possible to decide whether a given geometric structure such as line, curves etc is present or not in each digital image and one can give a suitable model for object recognition.

1.2. Problem statement

- Remote Sensing image analysis uses spectral information on a pixel by pixel basis. This captured information on the cell and information about patterns surrounding the pixel of interest often provides useful supplementary information. Usually human visual interpretation performs pattern recognition better than state of art computer algorithms. Availability of sophisticated instruments to acquire data at high resolution and in different spectral channels improved the information contents when more than one bands are used. Most of experiments performed by Gestalt psychologist were based on grey level digital photograph which contains little information while in remote sensing image analysis the automatic processing using multispectral images is preferred because of huge amount of data that often has to be analysed.

- Recently proposed algorithms based on Gestalt principles perform well on general image analysis. In geo-information where we use different type of images that have different nature, different pattern and different number of bands etc, usually requires a robust algorithms which are capable in extraction of meaningful information for general image application. In consideration to this research it is not clear whether the algorithms based on Gestalt principle will apply or perform well on remotely sensed images.

1.3. Research Identification

1.3.1. Research objectives

The main objective of this research is to add a new method in remote sensing image analysis by adopting an existing algorithm based on Gestalt principles in interpretation of multispectral images. This can be described using the following sub-objectives.

1.3.2. Specific research objectives

- Implementation of algorithms based on Helmholtz principles to remote sensing images
- Identification of basic grouping laws that can be used for image detection
- Selection of parameters to be involved in an algorithm that based on Helmholtz principles for analysis of image

1.3.3. Research questions

- How do algorithms based on Gestalt principles apply to remotely sensed images?
- How can Gestalt grouping laws be applied for feature detection in remotely sensed image?
- How can the best threshold values of parameters be found and involved in an algorithm based on the Gestalt principle for feature detection in remotely sensed images?

1.4. Innovation aim at

The innovation of this research aim at adopting one of the existing algorithms based on Gestalt principles of visual organization in extraction of information using multispectral images.

1.5. Outlines of the thesis

The research adaptation has been grouped into seven chapters on which chapter one gives the general review on remote sensing image acquisition, the background on Gestalt theory and the objective of research. Chapter two gives a concise description on the theories and principles. It also reviews the literature which has been used in standard feature detection of remote sensing images. Chapter three introduces the case study area and type of data used in this research and the method used in image processing concepts on validations are discusses on chapter four. Chapter five discusses on the results due to implementation of the Helmholtz principle to multispectral images. Chapter six described the general discussions and the summary on the conclusion and recommendation is given in chapter seven.

2. Literature review

This chapter provides a brief overview on the Gestalt theory and principle in visual interpretation of feature in digital images. Also it addresses the basic principle of perception due to Helmholtz and its related works. Finally it summarises on the proposed methods to validate the line segments detected from different digital images.

2.1. Gestalt theory

The origin concept of Gestalt theory was first introduced in contemporary philosophy and psychology by Christian von Ehernfels in his famous work (Uber Gestaltqualitaten) on the Quality of form in 1890 [13]. Ehrenfels was a musician in his work on Gestalt Qualities he pointed out that a melody is still recognizable when played in different keys, even though none of the notes are the same, and that abstract form attributes such as squares, angularity which can be conveyed by a wide range of specific elements. From this notion, Wertheimer argued that if a melody and the notes that comprise it are so independent, then a whole is not simply the sum of its parts, but a synergistic "whole effect," or gestalt[14]. The great significance of the work of Ehrenfels from the point of view is the ability for developing a theory of dependence, the implications of which were to extend far beyond the narrow sphere of perceptual psychology.

The consistence of idea on Gestalt theory has unique contribution which insisted that ‘Gestalt’ is perceptually primary, defining the parts of which it was composed, rather than being a secondary quality that emerges from those parts [15]. Early 20th century theorists, such as Kurt Koffka, Max Wertheimer and Wolfgang Kohler saw objects as perceived within an environment according to all of their elements taken together as a global construct. This 'gestalt' or 'whole form' approach sought to define principles of perception [16-17]. This principle seems to be a natural mental law which determined the way in which objects are perceived and took several forms, such as the grouping of similar objects together within the global process. Gestalt through its descriptive method, has formed the basis for much further research in the perception of patterns or objects behaviour into thinking and problem solving [9].

2.2. Quantitative Gestalt theory

The quantitative aspect of Gestalt theory allows the translation of Gestalt grouping laws into automatic computation of gestalt in digital images [9]. This computational, systematically use of statistical approach in modelling explicitly those properties (partial gestalt) that appears to support its information processing capacities. In a real sense such a modelling are represented as algorithms for achieving some results using computer understanding [18]. In order to facilitate perception theory for computing partial gestalts, grouping becomes the main process in visual perception.

2.3. Gestalt grouping laws

Gestalt grouping laws are the main process in visual perception and aim to formulate the regularities according to which the perceptual input is organized into unitary forms [19]. These laws appear to guide the organization of elements into perceptual groups and demonstrate on how our sensation are organized and interpret the world when perceive complex scenes composed of many groups of objects on some background [20].
In order to interpret what we receive through our senses different grouping laws attempt to organize this information into certain groups. Among the Gestalt grouping laws include the similarity, proximity, continuity, and closure [9].

2.3.1. The law of similarity

This grouping law refers to the tendency of our perception to group things together based upon those similar elements that share qualities (such as colour, size, or shape) and perceived as part of the same form [21]. For example in figure 2.1 the left image shows a sheet of evenly spaced light grey squares that can be perceived, but two squares are perceived as different from the rest and from each other.

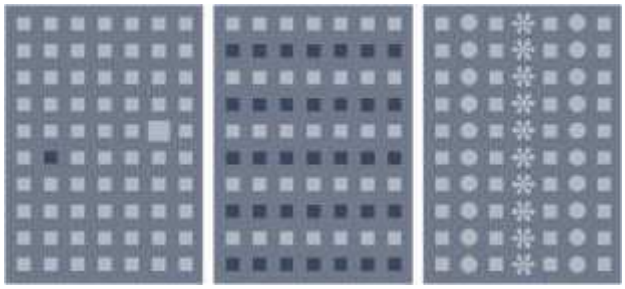

Figure 2.1 Law of similarity (http://www.infovis-wiki.net/index.php?title=Gestalt_Laws)

The left-middle square seems different because of its colour, and the right-middle square seems different because of its size. In the middle image, rows appear because we associate similar colours together even though the squares are evenly spaced. In the right image, columns appear because similar shapes are associated together.

2.3.2. The law of proximity

This law groups equal objects because of how close they are to each other. Figure 2.2 illustrates the law of proximity which tend to perceive elements to be associated when they are close to each other [21].

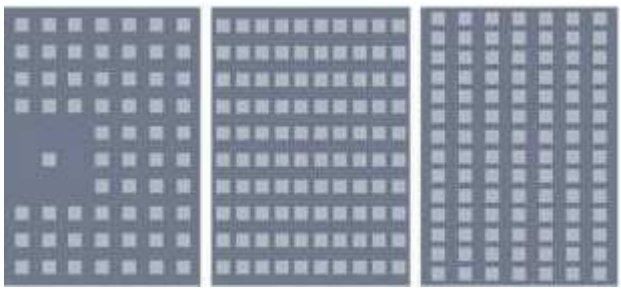

Figure 2.2 Law of proximity (http://www.infovis-wiki.net/index.php?title=Gestalt_Laws)

For example, the left image shows one square standing out among a sheet of evenly spaced squares. The lone square seems different because it is far away from the others. In the middle image, we perceive rows made from the same squares because there is less horizontal space between them than vertical space. The opposite is true in the right image, and so we perceive columns.

2.3.3. The law of continuity

Continuity or good continuation refers to the tendency to perceive things or patterns as they belong together in continuous form [21]. Figure 2.3 shows different groups of smooth and continuous pattern of contours that tend to be grouped together.

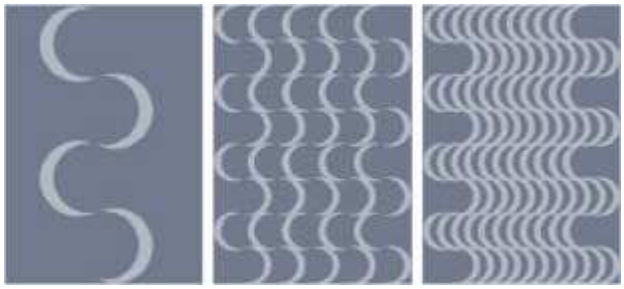

Figure 2.3 Law of continuity (http://www.infovis-wiki.net/index.php?title=Gestalt_Laws)

In the left image, for example, we perceive a continuous image of a wave, rather than alternating crescent moon shapes. The middle image emphasizes on the wave effect when the crescent shapes are reduced and repeated, such that a series of waves are perceived and not an individual wave or interacting shapes. Overlapping the same elements in the right image creates a continuous ribbon of pale grey waves that is either shallow or deep, depending on where we perceive the continuous forms.

2.3.4. The law of closure

The law of closure demonstrates the tendency of completing familiar objects that have gaps in them [21], for example figure 2.4 allows to group elements together or to interpret forms as complete though parts may be missing. In the left image, closure predicts that two diamonds are perceived and a half-diamond on the upper (rather than two X's and a half -X on bellow).

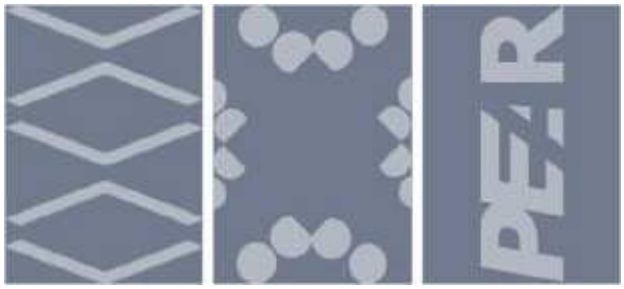

Figure 2.4 Law of closure (http://www.infovis-wiki.net/index.php?title=Gestalt_Laws)

Similarly in the middle image, a square appears to be sitting on top of a pattern of circles. Dark square is perceived and for the same reason the word "PEAR" in the right image is seen. Both the square and the "A" are not drawn, but each image is perceived complete with element even though some parts are missing.

2.4. Computing partial Gestalt in digital image

In digital images the basic grouping laws that group points which share some geometric quality are partial gestalt. These grouping laws are like vicinity and similarity which aim to build up partial gestalt to form a series of connected pixels along a certain region [22]. Helmholtz principle allows to compute any partial gestalt obtained by grouping laws [9] and a good example on which the computation can be applied to partial gestalt includes alignment, boundaries, cluster, grouping by orientation, size or grey level [9].

2.4.1. Discrete nature of digital image

From the point of view due to gestalt law the discrete nature of the digital image makes it necessary to redefine elementary geometrical properties such as distance, slope of the line and coordinates transformation which involves translation, rotation and scaling. These quantities are required for the definition and measurements of geometric parameters of object in digital images [23]. Digital image contains a finite number of grey level values on a grid. The information content to each grid according to Shannon's theory is bounded and the resolution of an image is finite [9]. Defining the digital local information as a function of u at a grid point $u(x, y)$ gestalt build up discrete nature of digital image in the expression of Taylor expansion by assuming that

- for blurry image at function u the value u(x, y) at each point is valid only if this value is close to (x, y)
- the gradient of u at each point is a vector given by

$$\Delta u = \left[\frac{\partial u}{\partial x}, \frac{\partial u}{\partial y} \right] \tag{2.1}$$

- the gradient direction is given by

$$\theta = \tan^{-1}\left(\frac{\partial u}{\partial x}, \frac{\partial u}{\partial y} \right) \tag{2.2}$$

- the gradient direction for the edge at $u(x, y)$ is given by

$$\theta_{edge} = \tan^{-1}\left(-\frac{\partial u}{\partial y} / \frac{\partial u}{\partial x} \right) \tag{2.3}$$

The local information that can be perceived in the image is described by the vector at each point and is tangent to the boundaries. The direction is invariant when the image contrasts changes.

2.4.1. Gestalt similarity principle

In section 2.2 the similarity law was introduced for those points having one or several features in common are being grouped. The gestalt grouping law considers alignment as the main partial gestalt where the objects are grouped by orientation or grey level values by assuming that are independent and identically uniform distributed in the random noise [20].

2.5. General detection principle

This principle is the perception principle called Helmholtz principle which introduces a method for computing geometric structures in a digital image by controlling both false positive and false negative [9]. In this principle the perceived meaningful geometric structure in the digital image have a very low probability to appear in a random noise [20], in this context, geometric structures are characterized as large deviations from randomness [9]. Helmholtz thought that if the probabilistic estimate is done in digital image then the proper prior model used to estimate the number of expectations must be known, for that case the possibility of loosing any generality in the approach is greater unless the probabilistic model could be proven to be the right one for the image under consideration. Therefore the use of statistical estimates without any image model was proposed and yielded computational grouping thresholds associated with each gestalt quality [20]. Figure 2.6 illustrates the Helmholtz principle for which the non casual alignment was automatically detected as a large deviation from randomness. Consider top left, 20 uniformly randomly distributed dots, and 7 aligned points were added. The perceived meaningful alignment is detected as a large deviation. But at the bottom when the same alignment is added to 80 random dots, the alignment is no more perceived.

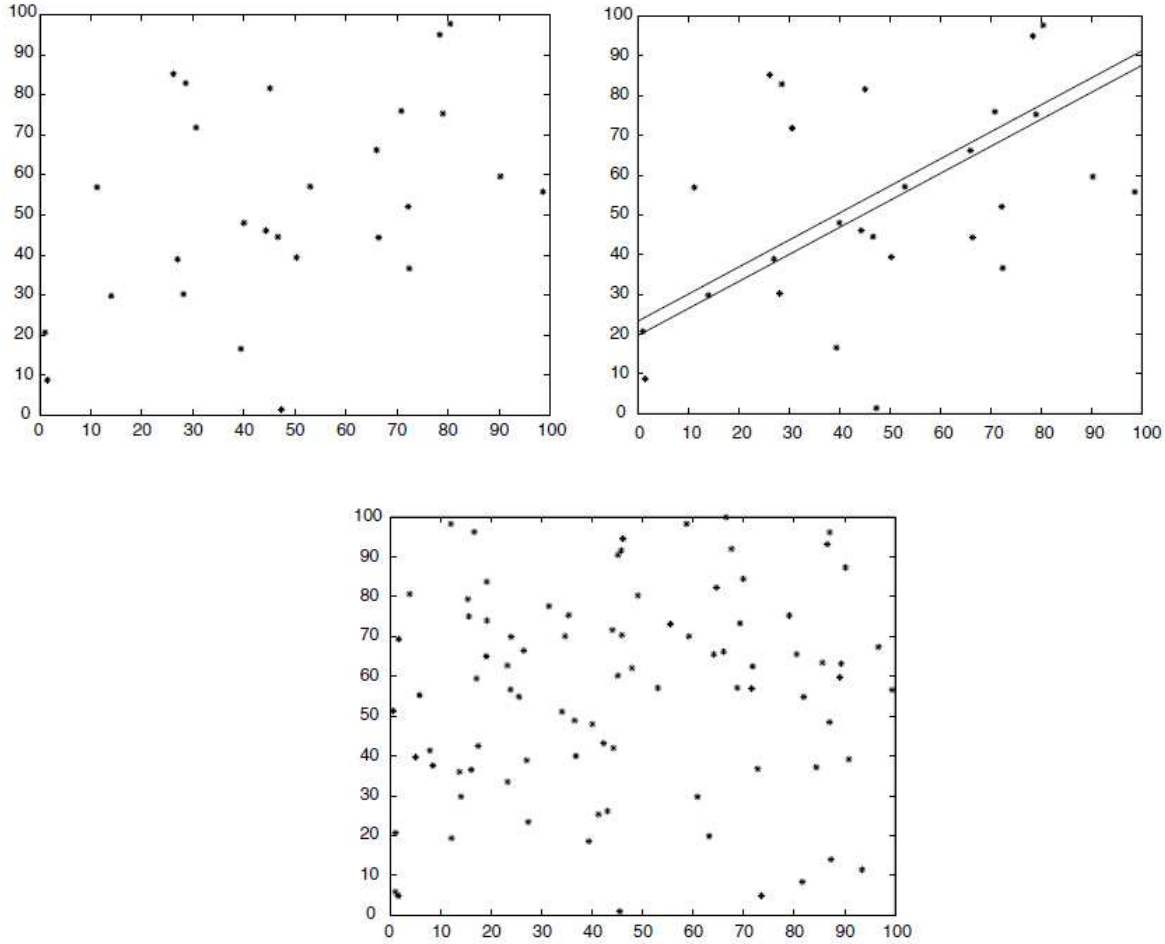

Figure 2.5 Illustration of Helmholtz principle (source [9])

2.5.1. Detections of alignments

Alignments in digital image correspond to a segment where the gradient can be observed orthogonal to the segment's direction [9]. Gestalt psychology considered alignment as the main partial gestalt to

which similar elements can perceived as a continuous form. Images are blurry, noise and alias in nature therefore by taking measurement at each pixel of the images for higher expectation of good accuracy is difficult. In order to detect these alignments, a detection threshold which tells whether a configuration of points may arise in the image is required[18]. In most cases these detection thresholds depend on a prior four basic parameters which are total length *l*, number of observed point in the alignment *k*, the precision of alignment *p* and the size of the image *N*. These parameters may define a line segment in the image as a straight line where many of its points share the same gradient angle up to a certain tolerance.

2.5.2. Parameters in digital image processing

In statistics or mathematical science a parameter also called an auxiliary measure is a quantity that defines certain characteristics of systems [24]. That is parameter can be a special kind of variable that refers to data that a subroutine or subprogram receives on which to operate. In different contexts the term may have special uses[25]. The semantics for how parameters can be declared and how the arguments get passed to the parameters of subroutines are defined by the programming language, but the details of how this is represented in any particular computer system depends on the calling conventions of that system.

The perceived configurations in digital images according to Helmholtz principle may be detected by computer algorithms if the detection threshold ρ on the gradient magnitudes, tolerance angle τ, and detection threshold epsilon ε computed from $k_{min}(l, p, N)$ is minimum [9]. For the discrete segment with the point aligned on it the parameter will include those observed point *k* which is truly aligned and the total number of alignment *l* in the image of size *N*. Parameter simplify or change the representation of an image into something that is more meaningful and easier to analyze. In digital image processing is typically used to locate objects and boundaries such as lines, curves, etc.

2.6. Implementation of Helmholtz principle

In image analysis one of the main problems is the choice of adequate prior. Different methods have been introduced in order to improve the methods of extraction of information using different classical methods. For example in the Bayesian model where the aim is to find the original model, if the given observation is '*D*' by computing the maximum a posterior (MAP), the model is given by

$$\Pr(M|D) = \frac{\Pr(D|M) \cdot \Pr(M)}{\Pr(D)} \qquad (2.3)$$

The key data-dependent term $\Pr(D|M)$ is a likelihood that also called the evidence for the model, the term $\Pr(M)$ is the prior and always has to be fixed, in normal condition it is difficult to find a good prior for the given class of the image but if it is evaluated correctly, it is the key to Bayesian model comparison. This prior plays the same role as a regularity term in the variation framework so it is impossible to give all purpose prior [26].

According to Helmholtz principle any noticeable structure in the image is perceptually meaningful as exceptional to the randomness provided that this large deviation from the randomness corresponds to a prior fixed list of geometric structures. In this principle a prior geometric model is qualitative rather

than being quantitative [9]. In detection of linear feature, the main idea is to count the number of aligned points and detect line segments as outliers of non structured model as shown by figure 2.5. Considering the image to have objects, $O_1, O_2, ..., O_n$ which are independently and identically distributed random variable, and if the aim is to group those objects with connected pixel that share some common quality *K* then the quality groups of pixel for each group say $G_1, G_2, ..., G_K$ have a certain number of objects.

If the grouping process proves the a contrario approach, under the independence assumption the probability that at least *k* objects out of observed *n* at a precision *p* have a quality is given by the binomial distribution expressed as

$$B(n,k,p) = \sum_{i=k}^{n} \binom{n}{i} p^i (1-p)^{n-i} \qquad (2.4)$$

Now if $Nconf$ are different number of configuration to be tested, then the total number of events could be considered being meaningful if,

$$NFA = Nconf \cdot B(n,k,p) \leq \varepsilon \qquad (2.5)$$

Where:

$\varepsilon \leq 1$, for ε -meaningful

p = precision

n = size of the image

i = *k* number of observation from *i*=1

NFA is the Number of False Alarm of an alignment which is a smallest value of ε

2.7. Line segment detection

2.7.1. Megawave2 software

Megawave2 software is a free Unix/Linux package which aim at making the coding of signal and image-oriented algorithms easier[27]. An algorithm is implemented as a function written in C or C++ language. Megawave2 package are made up of the following

- Library of image processing modules that contains, original algorithms written by researchers for contributing to the reproducibility on going research.
- A C or C++ preprocessor and a system library, that allows easy and fast development of new modules for which only the algorithms have to be implemented, then the inputs/outputs are automatically handled by the preprocessor, and a documentation (module syntax) is generated as well.

The designed environment for the megawave2 software requires the programmer to focus only on the algorithms and not on the pure computer problems[27].

2.7.2. LSD algorithm

The line segment detector (LSD) algorithm is inherent Burns et al., (1986) method and uses statistical models that based on a contrario approach in detection of line segment in digital images. This

algorithm requires no parameter tuning and gives accurate results and a controlled number of false detection to the all grey scale digital images that have been tested [28].
The LSD algorithm was designed to provide a good false detection control. The false detection control is based in automatically providing detection thresholds that prevent detections which could happen by chance in a non structured image. Figure 2.6 gives a result of the line segments detected that corresponds to straight structures in the image. The detection is roughly corresponds with the expected result.

Figure 2.6 Line segment detected by LSD algorithm (http://mw.cmla.ens-cachan.fr/megawave/algo/lsd/**)**

Also some experiment shows that in noise image the LSD algorithms can not detect a structure unless the image has been analysed at different scale by Gaussian sub-sampling. Figure 2.7 show a masked square that could not detected by algorithm and figure 2.8 shows a detected square after Gaussian sub-sampling for the noise if roughly removed.

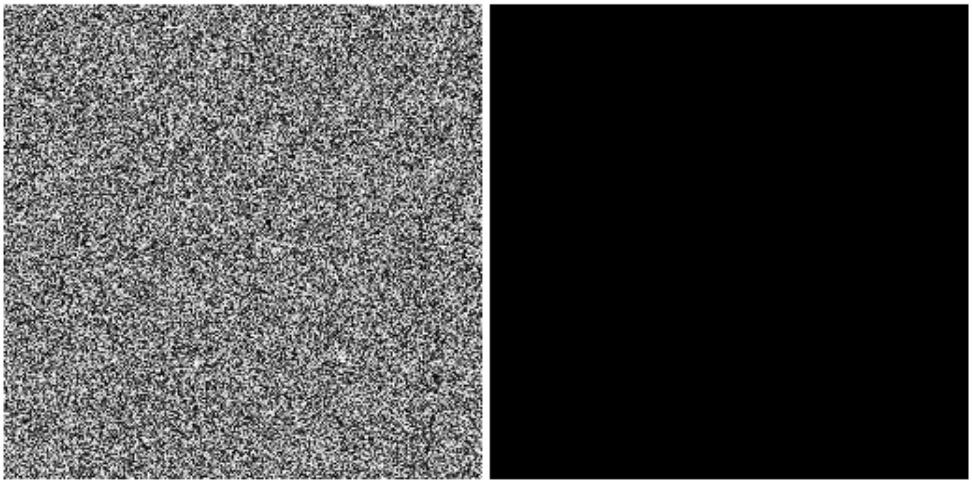

Figure 2.7 Undetected mask square in noise image (http://mw.cmla.ens-cachan.fr/megawave/algo/lsd/)

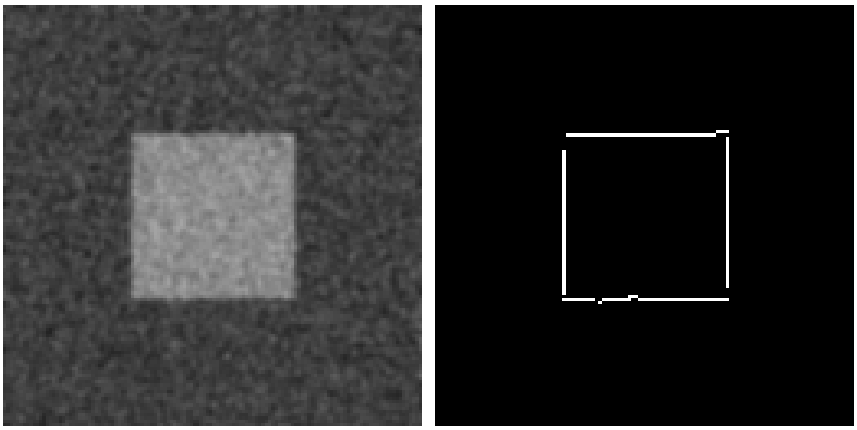

Figure 2.8 Detected square by Gaussian sub-sampling (http://mw.cmla.ens-cachan.fr/megawave/algo/lsd/)

2.8. Accuracy assesment

Information about the accuracy of available spatial datasets is an important part to any scientific research to ensure correct measurement can be performed from the resulting dataset produced either manually or extracted automatically from digital images [29]. Quality measures for spatial accuracy and completeness of the datasets has been suggested and explored by different researchers. For example in [30] and [31] they all suggest the use of epsilon error bands in some form to model the digitizing error of the position accuracy. In their suggestion dataset of higher accuracy are used for the assessment of the quality by the use of available GIS operations that work by establishing a number of buffers of increasing width around the lines of the reference dataset.
The accuracy and error in remote sensing arises when the statement of reliability of results is required to be understood and communicated [32]. In general when the accuracy objective is known it can be considered as an error but when otherwise it is considered as uncertainty. The uncertainty that exists in geographic data remains a problem if it is not explicitly stated and quantified for the user to evaluate its suitability in an intended application [33]. Since there is no specific method to asses the data extracted from multispectral images due to inherent uncertainty, two approaches will be introduced to evaluate the extracted information in this research. These include the buffer methods proposed in [34] and the visual examination method based.

2.9. Related work

The research on Gestalt principles has been growing and many methods have been proposed based on grouping laws. Most of implementation of these grouping laws had performed using gray level digital photographs or synthetic objects that contain little information. For instance, G. Kanizsa and M. Wertheimer performed an experiment on detection of regular curves in digital images, this experiment they found that in a computer vision the regularity guided by the law of continuity was often a property that satisfied by shapes of contours[20]. During their studies they proved that these laws were grouping laws such that object were seen when composed of an element sharing one or several common properties. The same theory were written by Desolneux, Moisan and Morel of which the object properties they called partial Gestalt [9].

Leclerc [35] attempted to define visual perception in terms of simplicity of description. He emphasized the idea that simplicity of description is an important guiding principle in computer vision

and used minimal-length-encoding to express this notion to perform image segmentation, data clustering and object recognition [36]. This law of simplicity is also known as the law of good figure. In remote sensing according to this principle, prior information about the earth surface and image sensor is incorporated in the language used to describe the world and sensor, and the inference process is to find the simplest description in the way that exactly reproduces the given images. Other experimental includes closure law which lead us to perceive an object as part of surrounded by a closed contour.

W. S. Geisler and Jeffrey S Perry conducted the same experimental studies on how the law of closure is sensitive and they provided an evidence that closed contours are easier to detect than open contours in the distributed random noise[37]. Another related work is Wertheimer principle which states ‘image interpretation does not depend on actual values of the gray levels, but only on their relative values’[9]. This principle was applied by Matheron and Serra who noticed that the level lines of an image contains the shape information, which are independent of the contrast information [38].

3. Study area and Data used

This chapter discusses about the study area and the data that are used in this study on which the performance of proposed LSD algorithm will be tested. Section 3.1 gives details on the study area and section 3.2 describes about the data characteristics.

3.1. Case study Area

The test site for this study is located in the central part of Netherlands around the Ketelmeer area. It covers an area of approximately to 14.7km x 15.0km, the position of an area in RD coordinate system ranges between 173120.018m to 187881.267m north and 506187.808m to 521218.831 east. In general the area is characterised with different patches of agriculture surrounded by water channels or polders including the narrow path distributed over the region. Few objects such as line strips, electric lines are also found. Figure 3.1 gives the location of the study area.

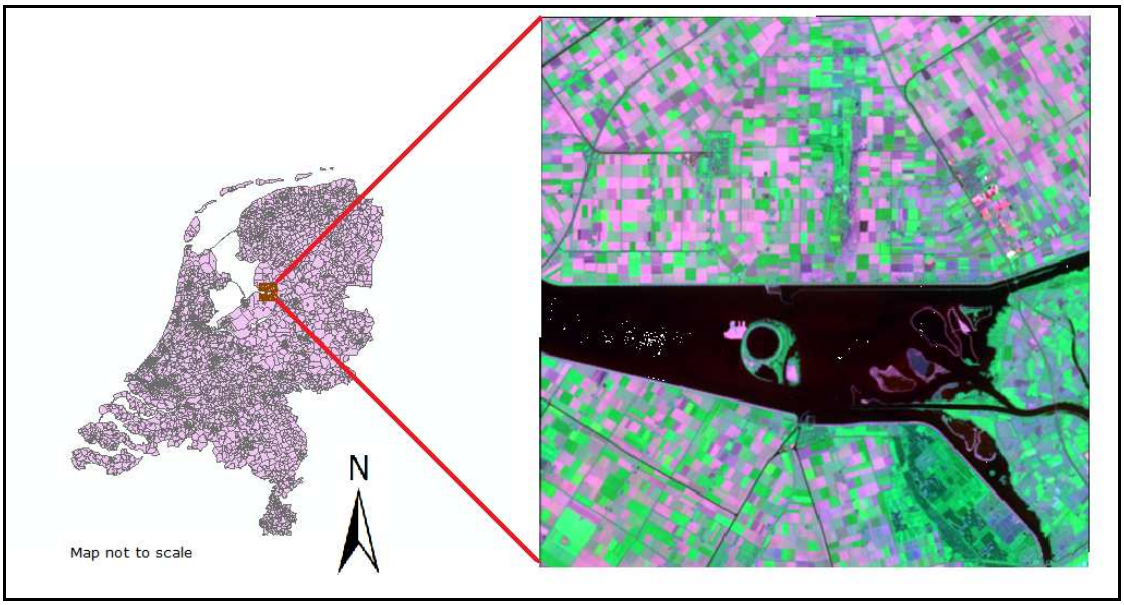

Figure 3.1 Study area

3.2. Data

In this study the data has been characterised into two types. The image data from Landsat7 ETM+ and GeoEye and the topographical map which is described as TOP10 vector map.

3.2.1. Image data

3.2.1.1. Landsat7 ETM+ Image

The ETM+ is a multispectral scanner, earth resources sensor designed to achieve higher image resolution. This sensor, images a swath of 185 km (115 miles) wide, but each pixel represents a 30 m x 30 m ground area, except in the case of the far-infrared band 6, which uses a larger 60 m x 60 m pixel. The Landsat7 ETM+ sensor has seven bands that simultaneously record reflected or emitted

radiation from the Earth's surface. Table 3.2 illustrate the band sensitivity to a certain feature characteristics and Table 3.1 summarises a general characteristics of the landsat image.

Launch Date	15 April 1999, at Vandenberg Air Force Base in California
Orbit	705 +/- 5 km (at the equator) sun-synchronous
Orbit Inclination	98.2 +/- 0.15
Orbit Period	98.9 minutes
Grounding Track Repeat Cycle	16 days (233 orbits)
Resolution	15 to 90 meters

Table 3.1 landsat image characteristics

Since the remote sensing image involves the measurement of reflected or emitted electromagnetic energy it was necessary to study the property of bands in relation to the spectral characteristics of features to be detected from the image. The seven spectral property performed by landsat sensor is summarised in table 3.2 describing the major advantage on the use of the respective band.

Band	**Region**	**Wavelength (μm)**	**Major Application**
1	Blue	0.45-0.52	Separation of soil and vegetation
2	Green	0.52-0.60	Reflection from vegetation
3	Red	0.63-0.69	Chlorophyll absorption
4	NIR	0.76-0.90	Delineation of water bodies
5	MIR	1.55-1.75	Vegetative moisture
6	TIR	10.4-12.50	Hydrothermal mapping
7	MIR	2.08-2.35	Plant heat stress

Table 3.2 Spectral band characteristics

3.2.1.2. GeoEye Image

Geoeye operates its own fleet of Earth observation satellites, which provide visible and near-infrared images of land and sea at resolutions below 1 m. Its principal asset is the IKONOS satellite available high-resolution imagery at 1 m panchromatic and 4 m for multispectral images. The Geoeye satellite has four bands, band 1, 2 and band 3 for multispectral imagery and band 4 panchromatic. In this study band 1, 2 and band 3 are used. Table 3.4 summarizes the general characteristics for the image.

Launch Date	September 6, 2008, Vandenberg Air Force Base, California
Spatial Resolution	1 meter pan and 1.65 meters multispectral
Orbit	705 +/- 5 km (at the equator) sun-synchronous
Orbit Inclination	98 degrees
Orbit Period	98 minutes
Grounding Track Repeat Cycle	3 days
Swath	15.2km
Altitude	684km

Table 3.3 Geoeye image characteristic

3.2.2. Topographic map

A topographic map characterized by large-scale details and quantitative representation of relief usually using contour lines [39]. Traditional definitions require a topographic map to show both natural and man-made features. The Canadian Centre for Topographic Information define a topographic map as ‘a detailed and accurate graphic representation of cultural and natural features on the ground’ [40]. Other authors define topographic maps by contrasting them with another type of map. Distinguish from smaller-scale "chorographic maps" that cover large regions, "plan-metric maps" that do not show elevations,[41] and "thematic maps" that focus on specific topics [39].

3.2.2.1. TOP10 vector data

The Netherlands TOP10 vector data is a country-wide vector map which covers around 1350 map sheets in New RD coordinate system compiled from photographic maps at a scale of 1:10000. Its vectors provide coded descriptions referring to a theme and possibly a classification for a specific area to be portrayed on the map[42]. These maps can be used to validate some geospatial information as they are produced at a better accuracy.

In this study, a vector map at a scale of 1:10,000 generated in 2002 from photographic map will be used to compare the validity of extracted line segment derived from landsat7 image by LSD algorithm.

4. Methodology

4.1. Geometric transformation

Geo-referencing refers to the process of referencing a map image to geographic location whereby image geometry is transformed into a mapping system of a given area [5]. Geo-referencing was done in ERDAS Imagine in which the first order polynomial geometric model was applied. Seven control points were used to georeference Landsat ETM+ image while six control points were used for GeoEye image. The overall accuracy of transformation was 0.0185 and 0.0106 for Landsat7 ETM+ and GeoEye respectively. Appendix A shows more details about the results on geometric transformations

4.2. Detection procedures

The detection algorithm proposed in this research is based on the perceptual principle which finds the line segment as an outlier of the non structured model. In this principle the aligned points whose gradient direction is approximately orthogonal to the line segment is considered valid and are detected [9]. In the first step, the algorithm partitions an image into the region for which each region consists of groups of inlier and outlier points. If the inliers are sufficiently enough to be connected they form a model that computes a line segment and if those inlier points are not sufficient no detection are made [43]. Figure 4.1 illustrates how the algorithm determines the inlier points in the search of line segment. The process is considered as a regional growing.

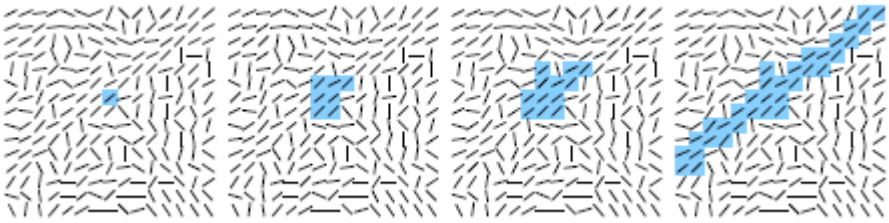

Figure 4.1 Regional growing of aligned points (source: [28])

The regional growing process is an iterative one, it connects all points with similar gradient angle until no new points are added[28]. Usually the pixel that added to the region has similar gradient orientation and is visited once so that it cannot be used as a starting point for the new region. During the growing process the rectangular described by the line support region is computed depends on two parameters (long enough and contrasted enough) which are fixed by a threshold in computer vision [9].

4.2.1. A rectangular region

A line support region gives a visual impression on how the set of pixel is associated with the line segment. Under a contrario assumption the direction and the position of the segment in the random noise is independent and uniformly distributed. The geometrical object of the line segment in the image is characterised by its end points and the widths[28]. The two end points give the length of the line segment. Figure 4.2 shows the parameter that describes a line segment.

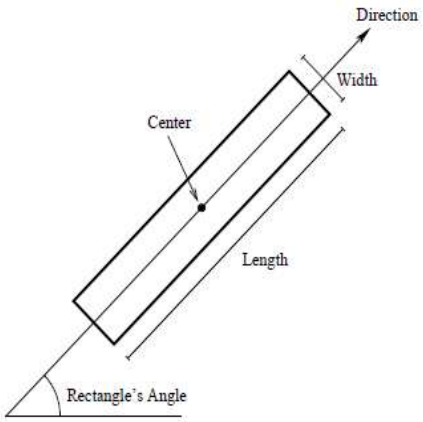

Figure 4.2 A line segment (source: [28])

The orientation of the level line is described by the use of the mean level line angle as the main direction of the contrasted line segment. In the proposed algorithm the centre of mass is used to select the centre of rectangle and the first initial axis to select the rectangle orientation[28]. The gradient magnitude is used as the pixel mass where the points with large gradient values correspond to the length of the line segment. The resulting orientation depends on the intensity contrast of the pixel, from low to high or high to low[9].

4.2.2. Gradient orientation

Alignment in digital image corresponds to the line segment where the image gradient is observed roughly orthogonal to the segment direction.

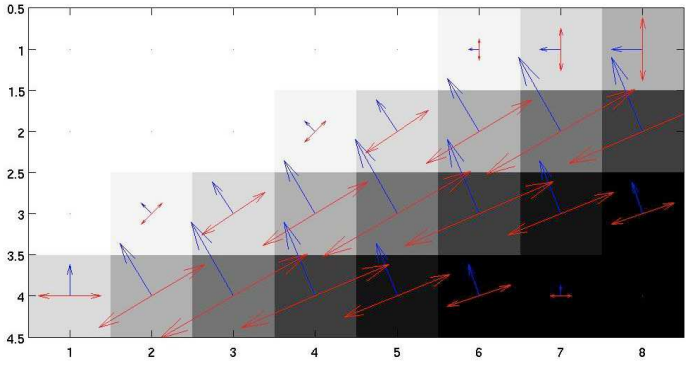

Figure 4.3 Search for maximum intensity (http://www.seas.upenn.edu/~cse399b/Lectures/CSE399b-04-edge.pdf)

Mathematically the image gradient is given by the derivatives of two variable functions (which are image intensity function) in the horizontal and vertical direction. At each point the gradient vector points in the direction of largest possible intensity increase (from dark to bright) and the length of gradient vector corresponds to the rate of change in that direction figure 4.3 describes.

Once the algorithm compute the length of gradient vector the threshold is used to decide whether the gradient orientation are present or not at an image point then for those points that certify the condition based on their length l, number of aligned points k are taken as valid detections along the line support region[28].

For illustration figure 4.4 described how the points may be considered as a valid detection at a given threshold criterion where the line segment shown has four aligned points among seven.

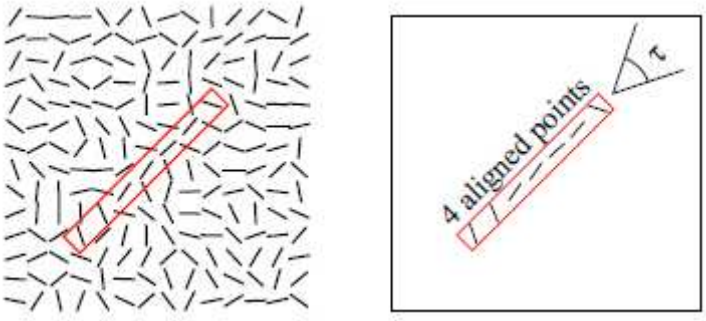

Figure 4.4 Aligned points along rectangle region (source: [28])

4.3. Line Segment Detection algorithm

The line segment detection algorithm simply LSD algorithm can be summarized by a complete pseudo code Algorithm bellow which consist subprograms.

Algorithm: LINE SEGMENT DETECTOR (LSD)

input: An image I, parameters ρ, τ and ε .

output: A list of rectangles.

```
1 ( LLAngles, GradMod, OrderedListPixels) ← Grad(I, ρ );
2 Status (allpixels)← NotUsed;
3 foreach pixel p in OrderedListPixels do
4           if Status(p) = NotUsed then
5           region ← RegionGrow(p, τ , Status);
6           rect ← RectApprox(region);
7           nfa ← NFA(rect);
8            nfa ← ImproveRect(rect);
9            if nfa < ε  then
10                Add rect to out;
11                Status(region) ← Used;
12          else
13                Status(region) ← NotIni;
14          end
15    end
16 end
```

The given subprogram in the LSD algorithm performs a specific task within a program.

4.3.1. Subprogram Grad

This program computes the image gradient and gives three outputs which are level-line angles, the gradient magnitude, and an ordered list of pixels. The parameter ρ is a threshold, points with gradient magnitude smaller than ρ are not considered. To construct the list that used to give a priority to pixels as seeds in the search of line-support regions, the pixels are classified into different orientations according to their gradient magnitude; the list starts with the pixels belonging to the orientation with

high gradient and ends with the pixels belonging to the low gradient. The list is roughly ordered in decreasing gradient magnitude order.

4.3.2. Subprogram RegionGrow

This program process the digital image by partitioning it into multiple lines of support region. The goal is to simplify and change the representation of an image into region that is more meaningful and easier to analyze. Pixels in an image that have the same label (such as colour, size and orientation) are connected together. The trend of growing seed is illustrated in figure 4.1.

4.3.3. Subprogram RectApprox

The program gives the approximation region where the probability of the line segment can occur. Figure 4.5 shows the final result of a rectangle that approximates the line support region.

Figure 4.5 Approximation of line support region (source: [28])

The best result of rectangle approximation is the one that gives the smaller NFA value.

4.3.4. Subprogram ImproveRect

This program uses the result from RectApprox subprogram to improve the approximated rectangle of the line support region to the best approximation. It tests the width and all lateral position variation. The width of the rectangle is very influential to the accuracy of rectangular approximation of line support region. In the line support region the error of one pixel wider adds many non aligned points to the length of the segment, results in increase of NFA value which may lead to non detection.

4.4. Parameter involved

Three parameters Scale, tolerance of level line angle and detection threshold epsilon have been involved in LSD algorithms for line segment extraction from the image.

4.4.1. Gradient tolerance angle

The tolerance of the level line angle group pixels into line support regions and is denoted by 'τ'. In LSD algorithm the tolerance angle used is computed from $180^{o}/d$ where'd' is a number of different orientation. The proposed default value is 8.0. Figure 3.3 illustrates how the line segment can be described in terms of its parameter. The tolerance gives the direction of the line segment.

4.4.2. Scale image parameter

The scale is denoted by'*s*' is a smoothing parameter that used in order to get a better representation and robust measurement can be performed in the image when the noise is filtered out and some texture in the image has been emphasized. Scale has an influence on the intensity of an image features change, therefore different objects in the image only may exist as meaningful entities over a certain ranges of scale[9]. The scale in the algorithm makes explicit relations between structures at different scales, and also makes image features stable over large ranges of scale. To avoid aliasing the algorithm uses Gaussian kernel, its derivatives as the only possible smoothing kernels. The proposed scale default value used is 1.0

4.4.3. Detection threshold epsilon

A line is composed of infinite number of points and the confidence limit for the region can be described by the detection threshold epsilon parameter denoted by '*e*' and is expressed as value = -log10 (max.NFA). The NFA measures the meaningful of an event and it reflect the probability value for which the smaller the value the more detection of the meaningful event is [9]. The default value for the detection threshold epsilon is 0.0.

4.5. Strategic feature extraction

This section shows several steps conducted to reveal the performance of the proposed LSD algorithm to multispectral images. The method has been implemented in C Language on megawave2 software which is compatible with Linux operating system. An experiment uses Landsat image. During the first stage of implementation the algorithm was run without tuning parameter that help to control the expected number of false positive in detection of image. The result was not satisfactory and this leads in selection of parameter that can be tuned in order to improve the results.

4.5.1. Parameter selection criteria

The criterion made in selecting parameter was based on LSD default parameters that were proposed after testing different digital grey value images. Table 3.4 shows the parameters and its default value

No.	PARAMETER	DESCRIPTION	DEFAULT VALUE
1	*s*	Image scale	1
2	*d*	Tolerance on the level line angle	8
3	*e*	Detection threshold epsilon	0.0

Table 4.1 Parameter default value

4.5.2. Feature extraction

Feature extraction involves simplifying the amount of resources required to describe a large set of data accurately that can help in object recognition. The extraction of feature where done using LSD algorithm that enables to process the image data depends on the parameter settings. The detection result is organised as a vector (x1, y1, x2, y2, w) where (x1, y1) describes the start of the line segment and (x2, y2) stands for the end of line segment and 'w' gives the width of the line segment. Also the results can be displayed as a binary image for visualizations. Figure 3.2 left shows the vector file and the right shows the binary image.

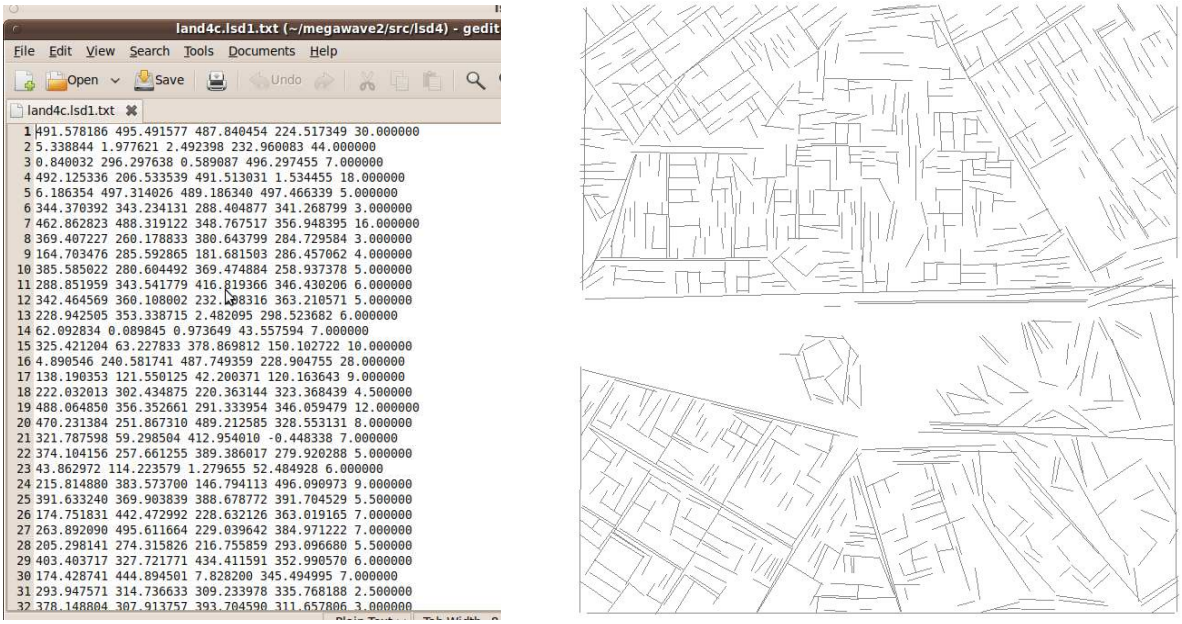

Figure 4.6 left organised vector data and right binary image

4.6. Statistical analysis of extracted linear feature

In analysing the results two approaches were consider in order to select a best set of data that can have a better extracted line segment using LSD algorithm. The first approach was to find the total number of line segment in the dataset and second approach was to find the total length of the line segment in the dataset. Then by using this concept each set of data were computed and the results have summarised in table 3.6 and table 3.7

4.6.1. Description of the line segment

A line segment extracted by LSD algorithm can be detected as a full line or part of line depending on the spectral strength of the pixel at the particular position for describing a line segment. The extraction can be influenced by the threshold value involved during implementation of an algorithm. Figure 3.8 describes two set of line segment of which four independent segments where extracted using different thresholds values. The observation after overlay on the original image two possible situations exist as shown in figure 3.8.

Figure 3.8a contains four sets of long segment while figure 3.8b contains four sets of short segment. The aim is to maximize the extracted features that correspond to the original image. In the process of overlay the extracted segment the sum of the line segment in figure 3.8b was not equal to the origin image. The overlay creates a gap which gives a significant insight about the effect of the parameters involved in the extraction of line segment in the image.

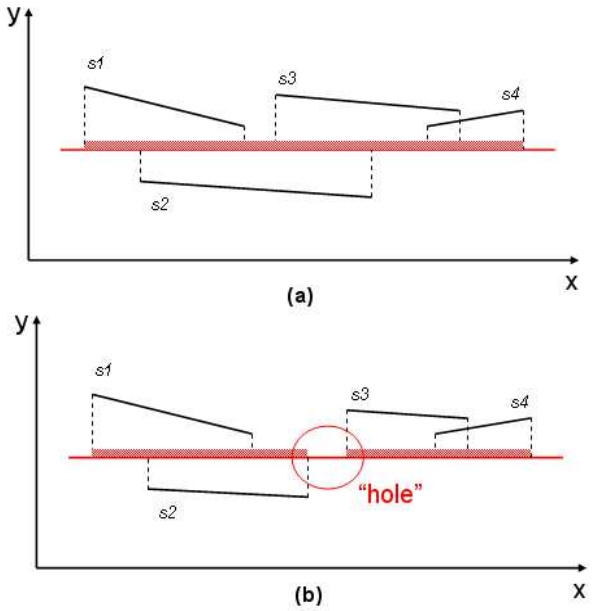

Figure 4.7 Comparison of extracted and original line segment

Figure 3.8a shows the complete set of line segment in relation to the original image. This gives a robust result for the parameter involved in algorithm during extraction of line segment. Similarly the computations in the following sections describe the same scenario.

4.6.2. Computing total number of line segment

In statistics the total number is given by the summation of all line segments present in the dataset. Recall to the set of data which described as a set of starting point (x1, y1) and ending point (x2, y2). The length of the line 'l' is given by

$$l_i = \sqrt{\left((x2 - x1)^2 + (y2 - y1)^2\right)} \qquad (4.1)$$

If N is the set of data contain 'l_i' length, then set of N is given by

$$N = (l_1, l_2, l_3 \ldots\ldots\ldots l_{n-2}, l_{n-1}, l_n)$$

The number of line segment in set N is given by counting each line present in the set. Such that if 1 implies the first line then the total number of N = n

In this counting does not matter about the length of the line segment each line is considered to have equal chance. The results for the number of line segment is summarized in table 4.3

4.6.3. Computing total length of line segment

The total length of line segment present in the dataset is defined by the summation of all individual length of line segments present in the dataset.

Now from equation 2 the total length of line segment is given by

$$L = \sum_{i=1}^{n} l_i \qquad (4.2)$$

Where L is the total length in set N

l individual length of line in set N

n is the number of lines in set N

The computations based on the total length of the line segment to each computed dataset is summarized in table C.2 appendix C

4.7. Concept of validation

The concept of validation can be expressed as the procedures of demonstrating the expected results of one or more dataset by referring to another set of data. It often includes two or more dataset to be compared for which one is used to control the spatial quality of the others [19].
In this part three datasets are chosen for line segment validation. Since in remote sensing image there is no specific method to validate the linear feature that are characterised as vector data. Two approaches have been done in this research to check the consistence of the meaningful extracted line segment from multispectral image by comparing the extracted dataset to the truth or reference dataset. The problem arises when choosing to which reference system the data will match as it is difficult to collect the proper reference dataset. Before the implementation of these approaches, it was necessary to have the data in the same coordinate system.

4.7.1. Pixel coordinate system

A digital images are described as a matrix, consisting of a certain number of rows and a certain number of columns of which denoted as N x M. A row has its orientation in a vertical direction, while a column is in a horizontal direction. The first row is always at the top and named row number 0. The first column is at the left most, and is named column number 0. The representation of two integers in row and column number is termed as pixel coordinate system whose origin is at top, left most corner. Figure 4.8 depicts the matrix index system for pixel coordinate identification.

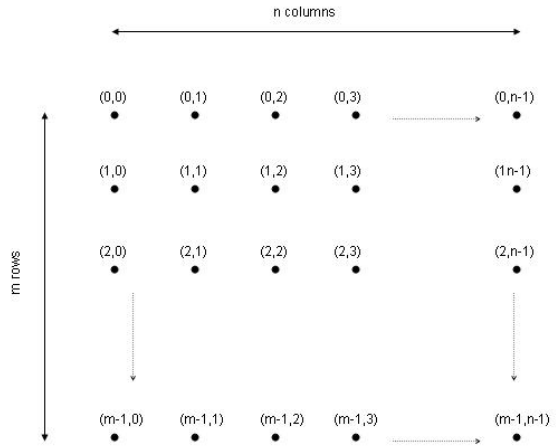

Figure 4.8 Pixel coordinate system (http://www.noobeed.com/nb_coord_system.htm)

4.7.2. Mapping coordinate system

In normal situation the mapping coordinate system refers to the right-hand coordinate system of which the origin coordinates is at the lower left and upper right corner of an image in such a way that spatial orientation as well as spatial scale is definitely defined. Figure 4.9 gives the relation of pixel coordinate system and the mapping coordinate system from which one can notices that rows in a matrix are parallel to the X-axis, and columns are parallel to Y-axis. The positive direction of X-axis is the same as that of column number but the positive direction of row number is opposite to that of the Y-axis.

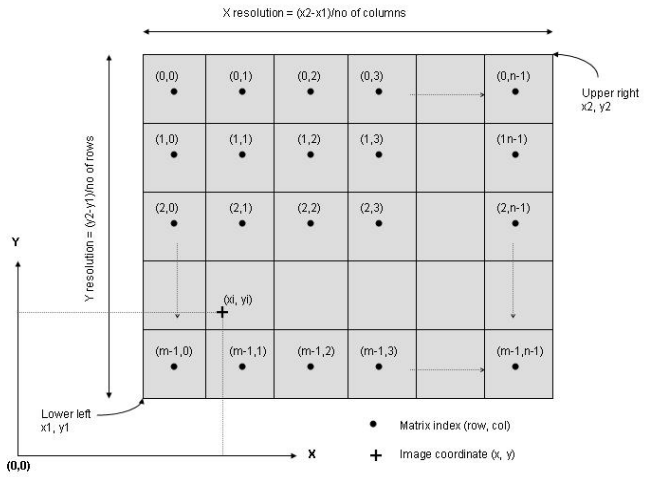

Figure 4.9 Pixel coordinates relation to mapping system (http://www.noobeed.com/nb_coord_system.htm**)**

4.7.3. Points to line conversion

The LSD algorithm produces a line segment in the form of points vector data that are organised as (x1,y1, x2,y2,width) in pixel coordinate system, where (x1,y1) is a starting coordinate system and (x2,y2) is the ending coordinate system. This coordinate system is closely related to the spatial coordinate system. The process of conversion of this system was done in Arcgis, using an extension called Hawth's tools that designed to perform spatial analysis. The conversion of point's data to line datasets using Hawth's tools requires only two sets of points in csv or dbf format to be joined as a line segment. In this case the format for the set of points are organised as (x1, y1, x2, y2).

4.7.4. Vector transformation

The transformation of vector data was done in Arcgis where the processing tool was performed by the use of spatial adjustment. This process allows integrating data that has no spatial reference into the geo-database by fitting it to the existing spatial data. In this research the reference image used is the landsat image in RD coordinate system. The process of transformation requires four minimum points which are well identified on both datasets. The displacement link is used to connect the source location (extracted dataset) to the destination location (reference dataset), at a minimum points the computations is automatically done and each displacement link the residual error is recorded in the Link Table and the overall RMS Error computed by the use of affine transformation is indicated. The transformation results shows that, land4a2 five control points were used and an accuracy of 0.2863 was obtained, for land6a2 four control points were used and an accuracy of 0.3378 was attained similarly for land8a2 five control point were used and an accuracy of 0.5629 was obtained. Detail results are shown in appendix B and the new coded name of the resulting dataset is given in table 4.5.

Code	**Parameter Involved**		
	No. of Orientation (d)	**Detection Threshold (e)**	**Scale (s)**
land4a2	4	0.0	2
land6a2	6	0.0	2
land8a2	8	0.0	2
land12a2	12	0.0	2
land16a2	16	0.0	2

Table 4.2 Geo-referenced codes names

4.8. Validation of extracted line segment

The method used in validation of the line segment depends on the data you have and the way it relates with the reference dataset. Two approaches in this research will be considered in validating a set of line segment. The first approach will use buffer method the concept proposed in[34], among of the methods proposed includes completeness, correctness and the quality. In this method matched datasets are derived from the intersection of the reference with the constant predefined width (buffer zone) with the extracted linear feature. Figure 4.10 illustrates the relationship referring to the road network. Since the reference dataset details are so limited the completeness and correctness will be taken into consideration during the process of validation.

Another approach is based on the use of visual examination of which the true measurement of an objects are taken directly from GeoEye image. The dataset of measurements are considered as a true reference and the comparison are made with the same objects extracted by the LSD algorithm. Different configurations of objects are selected from image for validation.

4.8.1. Matching procedure

Matched reference datasets are derived by intersecting reference with the constant predefined width (buffer zone) of extracted linear feature. The parts of the extracted data within the buffer are considered as matched figure 4.10 illustrates.

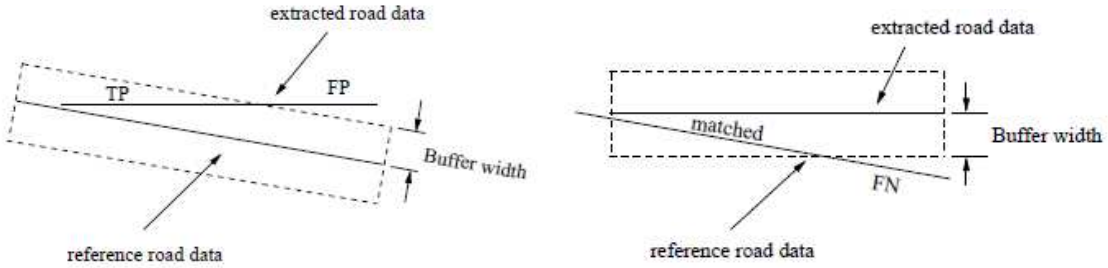

Figure 4.10 left matched extracted and right matched reference(source: [28])

In computations purposes the following linear feature characterization was applied,

TP= True Positive (matched extracted/reference data)

FP= False Positive (unmatched extracted data)

FN= False Negative (unmatched reference data)

4.8.1.1. Completeness evaluation

Completeness refers to the percentage of the actual present of the reference data that lies within the buffer around the extracted data. The computation is given by equation

$$Completeness = \frac{\text{Length of matched reference}}{\text{Length of reference}} \tag{4.3}$$

$$= \frac{TP}{TP + FN} \quad \text{(for low redundancy)}$$

Completeness ranges [0:1] that is its optimal value is 1

4.8.1.2. Correctness evaluation

Correctness refers to the probability of the correctly extracted data that lying within the buffer around the reference data. The computation is given by equation by

$$correctness = \frac{\text{Length of matched extraction}}{\text{Length of extraction}} \tag{4.4}$$

$$= \frac{TP}{TP + FP}$$

Correctness ranges [0:1] that is the optimal value is 1

4.8.1.3. Quality assessment

Quality refers to the goodness of the overall accuracy of the results as it takes into consideration the completeness and the correctness. Its computation is given by equation

$$Quality = \frac{\text{Length of matched extraction}}{\text{Length of extraction} + \text{Length of unmatched reference}} \tag{4.5}$$

$$= \frac{TP}{TP + FP + FN}$$

Quality ranges [0:1] that is the optimal value is 1

4.8.2. Buffer methods

In proximity analysis where position accuracy can be assessed by buffering method need the dataset that matched to each other so as to be able to compare them[34]. In this research the TOP10 vector data are used to determine the relationship between the extracted dataset by LSD algorithm and its corresponding neighborhood dataset. The zone that was established around map feature of the reference used to intersect a set of extracted data that linked to the location. Figure 4.11 illustrates by comparing a true coastal line and the coastal line to be tested.

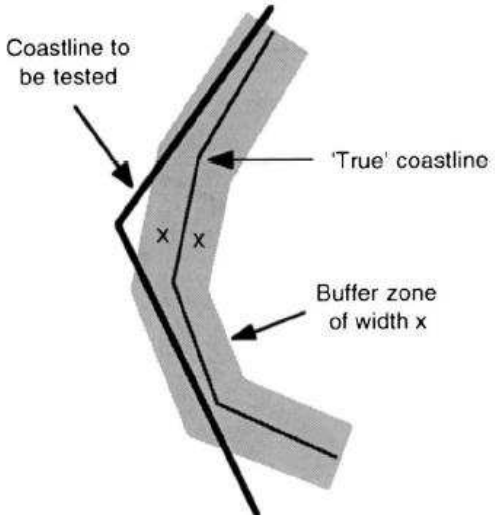

Figure 4.11 Buffer comparison (source: Goodchild & Hunter 1997)

Arcgis software enables to create a buffer along a point, line or polygon. Figure 4.12 and figure 4.13 show an example of the resulting matched dataset for land8a2 at different buffer width. The statistical results for the total length of matched datasets is presented in table 5.6

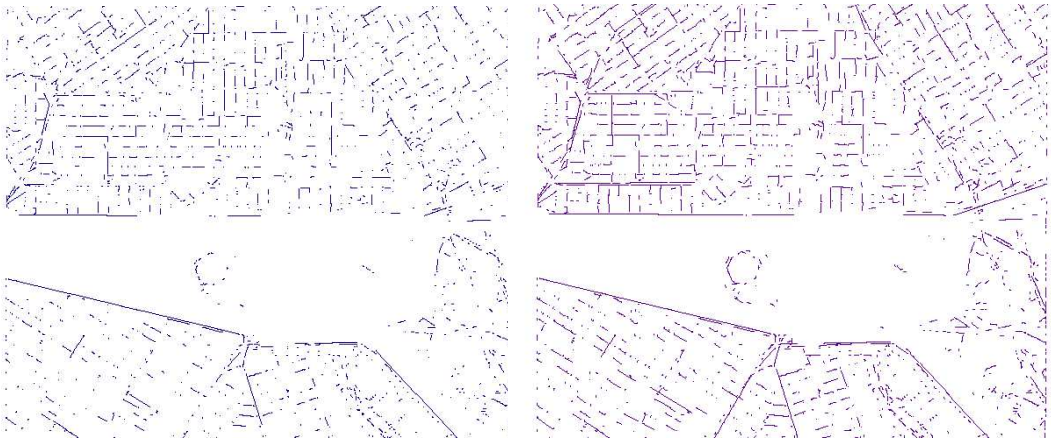

Figure 4.12 left buffer at 10m and right buffer at 20m

Figure 4.13 left buffer at 40m and right buffer at 60m

4.8.3. Visual examination methods

The second approach of validation involves those features selected from origin GeoEye image and used as a reference dataset. In this case 15 features as described in table 4.5 were identified in Geoeye image as shown in figure 4.14 and the measurement were taken as a true reference for comparison. In this validation the extracted dataset from landsat image that were detected by LSD algorithm are compared to the true reference to check the correctness of the LSD algorithm for remotely sensed image. For simplicity features are coded with field identification numbers (FID).

Figure 4.14 Selected objects from Origin Geoeye image

Based on the original image table 4.5 illustrates the field property that expected to be detected by LSD algorithm. The experiment was tested on three dataset of which the results is given in the following section.

Feature ID	Feature description
1	Double ditch
2	Line strips in agriculture area
3	Curved wide road
4	Line strips in agriculture area
5	A narrow cliff near the forest
6	A single ditch
7	A double ditch
8	Part of water surrounded by narrow part of Land
9	part of water surrounded by wide part of Land
10	A double ditch
11	Aanlst (Ferryboats)
12	Part of water surrounded by narrow and wide part of Land
13	Bicycle path in the forest
14	A double ditch
15	Part of pattern

Table 4.3 Description of the identified feature

5. Results

This chapter gives the experimental results obtained after applying different threshold value to the proposed LSD algorithm in search of optimal value that gives maximal meaningful line segment to multispectral image. All parameter that were involved as indicated in table 5.1 and their results were analysed. The detailed description of the results are summarised according to the effect of varying respective parameters which are tolerance of level line angle (d), scale of the image (s) and detection threshold epsilon (e).

5.1. Parameter setup

The main idea of setting different parameter thresholds was to obtain different variety of results from which the optimal threshold values can be chosen and added to LSD algorithm for other experiments. In feature detection the threshold value help to identify if the particular configuration of points is enough aligned to be detected as alignment from the image. The threshold values in this research were fixed manually as shown in table 5.1. Table 5.2 shows the total number of lines detected to each dataset.

Parameter included	**Tested values**
1. Tolerance angle (d)	16, 12, 8, 6, 4
2. Detection threshold (e)	0.0, 0.1, 0.01, 0.001
3. Image scale (s)	2.0, 1.5, 1.0, 0.5

	d = 16			d = 12			d = 8			d = 6			d = 4		
	d	e	s	d	e	s	d	e	s	d	e	s	d	e	s
a	16	0.0	2.0	12	0.0	2.0	8	0.0	2.0	6	0.0	2.0	4	0.0	2.0
b	16	0.0	1.5	12	0.0	1.5	8	0.0	1.5	6	0.0	1.5	4	0.0	1.5
c	16	0.0	1.0	12	0.0	1.0	8	0.0	1.0	6	0.0	1.0	4	0.0	1.0
e	16	0.1	2.0	12	0.1	2.0	8	0.1	2.0	6	0.1	2.0	4	0.1	2.0
f	16	0.1	1.5	12	0.1	1.5	8	0.1	1.5	6	0.1	1.5	4	0.1	1.5
g	16	0.1	1.0	12	0.1	1.0	8	0.1	1.0	6	0.1	1.0	4	0.1	1.0
i	16	0.01	2.0	12	0.01	2.0	8	0.01	2.0	6	0.01	2.0	4	0.01	2.0
j	16	0.01	1.5	12	0.01	1.5	8	0.01	1.5	6	0.01	1.5	4	0.01	1.5
k	16	0.01	1.0	12	0.01	1.0	8	0.01	1.0	6	0.01	1.0	4	0.01	1.0
m	16	0.001	2.0	12	0.01	2.0	8	0.01	2.0	6	0.01	2.0	4	0.01	2.0
n	16	0.001	1.5	12	0.01	1.5	8	0.01	1.5	6	0.01	1.5	4	0.01	1.5
p	16	0.001	1.0	12	0.01	1.0	8	0.01	1.0	6	0.01	1.0	4	0.01	1.0

Table 5.1 Parameter settings

Reading codes e.g. 1. Landd4a- the landsat image was tested when parameter d=4, e=0.0 and s=2
2. Landd12g- the landsat image was tested when parameter d=12, e=0.1 and s=1.0

code ID	d=16	d=12	d=8	d=6	d=4	sum
a	1137	1767	2551	2921	3057	11433
b	1205	1678	2186	2367	2344	9780
c	704	912	1069	1066	897	4648
e	1133	1762	2535	2908	3041	11379
f	1193	1663	2169	2354	2329	9708
g	687	906	1048	1038	885	4564
i	1135	1767	2543	2921	3049	11415
j	1205	1678	2186	2367	2344	9780
k	691	912	1058	1065	896	4622
m	1137	1767	2545	2921	3057	11427
n	1205	1678	2186	2367	2344	9780
p	704	912	1069	1066	897	4648
sum	12136	17402	23145	25361	25140	
Average	1011.333	1450.167	1928.75	2113.417	2095	

Table 5.2 Total number of line segments

5.2. Results based on parameter *d*

Parameter *d* describes the number of possible orientations that an algorithms uses in search of those points that share the common gradient angle. The algorithm uses the first order derivatives in computing the tolerance angle (τ) as described in chapter two section 2.3.1.

In the algorithm the tolerance angle used is computed from 180o divide by *d* as follows:

$$Tolerance\ angle(\tau) = \frac{180}{d} \qquad (5.1)$$

This implies that for *d*=16, tolerance angle is 11.25 degrees
for *d*=8, tolerance angle is 22.5 degrees
for *d*=4, tolerance angle is 45 degrees

Parameter *d* is among of the sensitive parameter to the LSD algorithm. By visual interpretation of the results figure 5.1 to figure 5.3 illustrates on the effect of varying parameter *d*.
Note. 1. Enclosed with blue colour, shows area with regular polygon i.e. Rectangles
2. Enclosed with red colour, shows area with complex polygon i.e. circle

In this research a line segment refers to a straight feature that connect group of points that share the same gradient angle to a certain tolerance. The effect of parameter *d* has been observed at different threshold values. The results as shown in figure 5.1 to 5.3 indicate that when parameter d increases the total number of lines detected decreases and the gaps are detected. This may imply that the algorithm in the search of connecting groups of points that share the same gradient angle for the feature with low contrast fail to connect the next point at low threshold value while it includes the next point for high threshold value. This can be observed in area enclosed with blue lines. From figure 5.1 right as the decrease of the tolerance angle the more the gaps in the image are found. The results to this effect are many gaps and few lines are detected at low threshold and long and many lines are detected at large threshold.

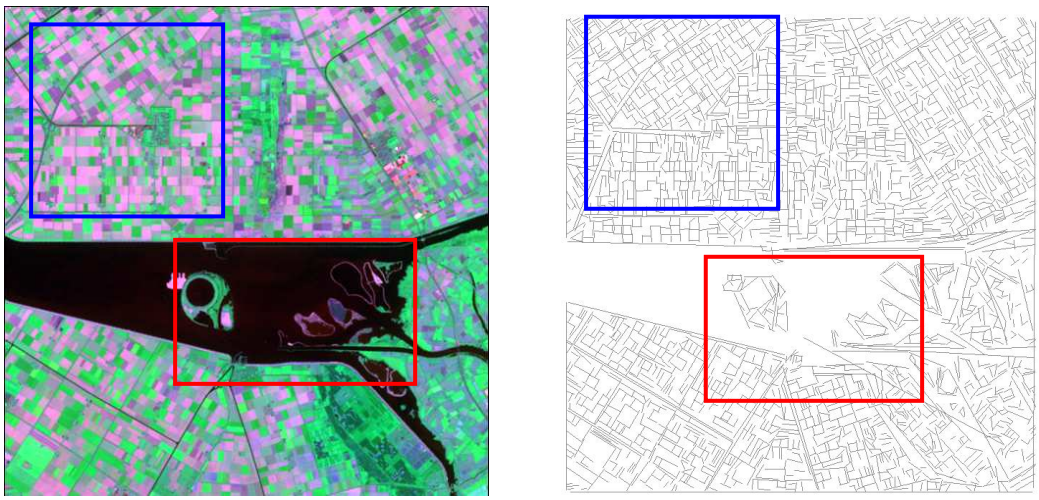

Figure 5.1 left origin image and right extracted image at *d*=4

Figure 5.2 extraction at *d*=6 and right extraction at *d*=8

Figure 5.3 left extraction at *d*=12 and right extraction at *d*=16

Figure 5.3 right image shows few line and many gaps when compared to the left image, and in figure 5.2 right image shows many gaps and few lines when compared to the left images. But figure 5.1 right

image give long and many line segments that closely corresponds to the original image in the left side. When consider the numerical value in table 5.3, it shows the average (Avg) number of the line segment and the average (Avg) length of line segment at different value of parameter *d*.

Figure 5.4 left shows the graph for the average number of lines detected and right graph shows the average total length when varying the parameter *d* respectively.

Parameter (*d*)	**4**	**6**	**8**	**12**	**16**
Avg. No. of Lines	2095	2113	1929	1450	1011
Avg. Total length	34270	29795	25025	17526	12245

Table 5.3 Average number of lines and total length

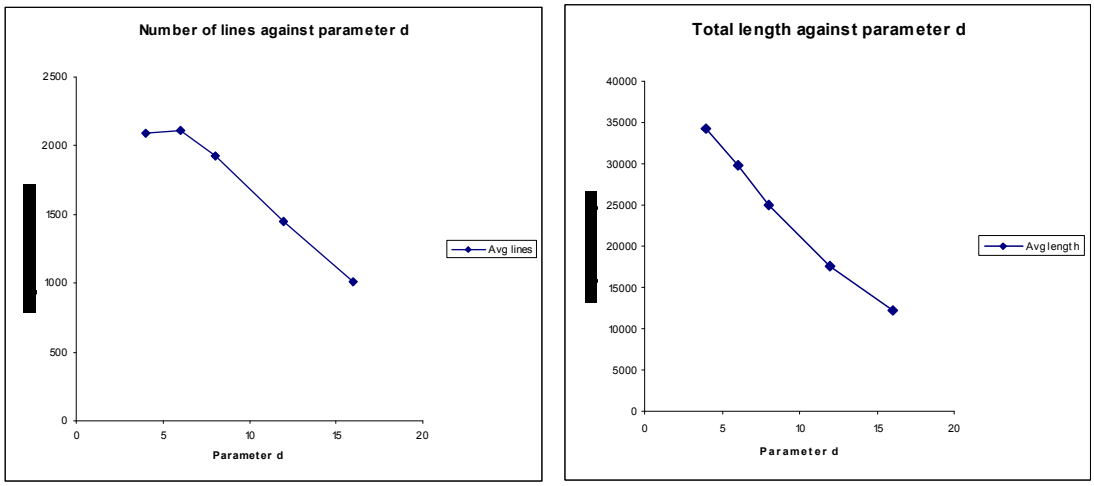

Figure 5.4 left shows average number of lines and right shows the Average length

The graph in figure 5.4 left shows the average number of extracted lines presents in the dataset. This graph shows the limit value where the number of lines is no longer extracting as parameter d tends to zero. Figure 5.4 right gives the rate of change of extracted feature in terms of length due to change of parameter *d*.

5.3. Results based on parameter *s*

Parameter *s* is the smoothing parameter that often uses to emphasize a certain feature by increasing the pixel intensity contrast. Table 5.4 is the summary of the results at different scale. The graph in figure 4.5 shows how parameter *s* is affected by the change of parameter *d*. The rate of change at a given scale depends on the value of scale used. For example table 5.4 when *s* is 2.0 and *d* is 4 many lines were detected and when *d* is 16 there is a rapid change of detection.

No.	parameter *d*	Number of Lines detected			Total length extracted		
		***s*=2.0**	***s*=1.5**	***s*=1.0**	***s*=2.0**	***s*=1.5**	***s*=1.0**
1	4	3057	2344	897	40902	37736	24272
2	6	2921	2367	1066	34067	32695	22745
3	8	2551	2186	1069	27567	27575	20063
4	12	1767	1678	912	17910	19502	15209
5	16	1137	1205	704	11765	13686	11376

Table 5.4 Number of lines and total length at fixed value e=0.0

But when one considers *s* to be 1.5, and *d* is 4 the rate of change of detection at *d* equals to 16 is not very fast compared to the first case. The same trend can be observed to the total length of line segment in table 5.4. If extra values for parameter *d* are added as shown in table 5.3, the graph in figure 5.5 indicates the possibility to estimates the optimal value of parameter *d* and parameter *s*. The observation from the table 5.5 shows that parameter *d* must be greater than one otherwise no detection can be performed by LSD algorithm.

Parameter *d*	Number of lines			Total length		
	s=2.0	*s*=1.5	*s*=1.0	*s*=2.0	*s*=1.5	*s*=1.0
1	0	0	0	0	0	0
2	739	506	129	22976	19112	10270
3	2624	1910	700	40228	36290	24019

Table 5.5 Trial value for parameter *d*

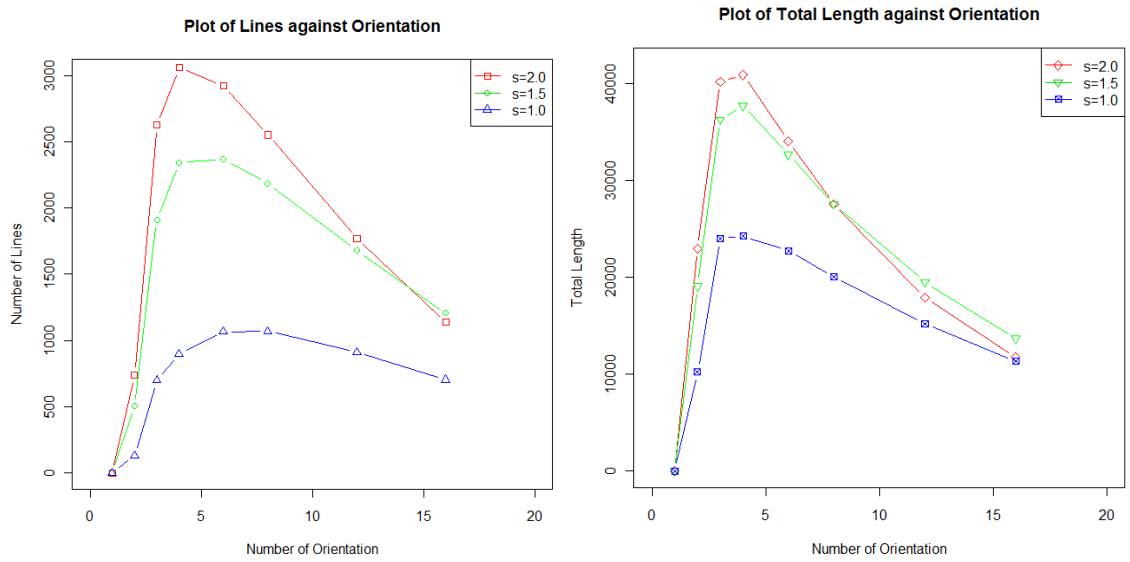

Figure 5.5 left number of lines and right total length when vary *d*

5.4. Results based on parameter e

Parameter *e* is the detection threshold epsilon expressed as a measure of maximum number of false detection. At minimal value of *e* the algorithm detects more refine lines. From table 5.6 it is observed that parameter *e* is invariant at a certain range of threshold. For example range between 0 and 0.1 it is difficult to detect the changes of the number detected by an algorithm. In order to detect the change

more values were added as appeared in table 5.6. The graph in figure 5.6 left shows that when *e* increases the number of lines detected decrease, which may imply that the increase of value *e* as a measure of precision causes non aligned points to be included in the line support region and those which qualified to be aligned are masked on it, as a results only few lines which are large deviation from noise are detected. Similarly the same applied to the total length of the line segments, the decrease of the number of segment results in the decrease of the total length of the line segment detected in the image.

Parameter e	Number of lines detected			Total length of lines extracted		
	d=4	d=8	d=16	d=4	d=8	d=16
0	3057	2551	1137	40902	27567	11765
0.001	3057	2545	1137	40902	27544	11765
0.01	3049	2543	1135	40858	27532	11750
0.1	3041	2535	1133	40808	27495	11735
0.5	3010	2487	1114	40588	27276	11650
1	2943	2431	1086	40182	27006	11534
1.5	2885	2390	1072	39841	26768	11474
2	2828	2344	1047	39461	26534	11349
10	2161	1762	766	34649	23099	9968
20	1558	1263	557	29169	19413	8644
30	1148	923	402	24868	16500	7410
40	847	677	258	21259	14072	6189
50	604	449	179	18216	11641	5449
60	428	321	135	15455	10119	4946
70	329	241	113	13499	8986	4651
80	271	190	96	12423	8101	4403
90	210	156	88	11110	7548	4314
100	165	129	71	10016	7027	3999

Table 5.6 Number of lines and total length at fixed *s*=2

The results due to parameter *d* shows no common rate of change in the number of lines detected within at a certain threshold value. For example rate of change of lines detected with parameter d when is 4 and parameter d when is 16 at threshold detection value 0.0 and 80, the graph of figure 5.6 left shows that the larger the tolerance angle the faster the number of lines decreases as you increase the threshold detection value and the smaller the tolerance angle the lower the decrease of the number of line segments detected.

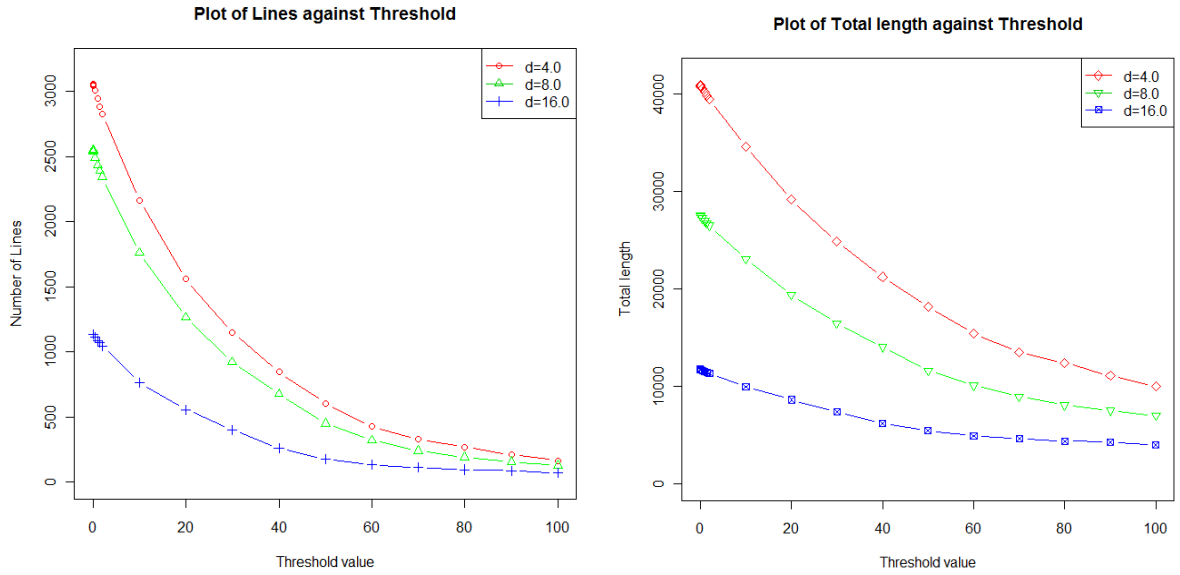

Figure 5.6 left number of lines and right total length against detection threshold

5.5. Results of extracted feature

5.5.1. Results based on Buffer methods

In this methods five dataset were experimented and the summary of the results, for completeness which shows the relationship between the matched feature and the reference dataset is given in table 5.7. Computations were done using equation 4.3 similarly table 5.8 shows the results for correctness which was computed using equation 4.4, correctness shows the empirical relationship between the matched feature and the extracted feature. At 3m buffer width was taken as a minimum width for testing the datasets. The results for the completeness was unsatisfactory compare to the proposed standards. This is an indication that either the reference dataset used contain feature that are not very closer to the extracted dataset. This result is shown in appendix D or the position accuracy of the extracted data is poorly defined. Figure 5.7 (right) describes the completeness of the dataset of which the minimum is 0.110 and maximum is 0.431 at a minimum buffer width of 3m while the optimal value for the completeness is one (1).

Buffer (m)	land4a2	land6a2	land8a2	land12a2	land16a2
3	0.431	0.429	0.305	0.178	0.110
5	0.448	0.449	0.334	0.187	0.116
10	0.484	0.490	0.375	0.213	0.131
15	0.506	0.525	0.406	0.239	0.147
20	0.522	0.548	0.427	0.256	0.159
30	0.551	0.578	0.457	0.291	0.175
40	0.568	0.602	0.472	0.302	0.185
50	0.581	0.608	0.479	0.308	0.200
60	0.587	0.613	0.485	0.311	0.202

Table 5.7 Completeness of the dataset

The results for the correctness at a minimum buffer of 3m is almost good compared to the completeness, the improvement in the results has caused by the decrease in the total length of extracted feature as it was computed using equation 4.4.

Buffer (m)	land4a2	land6a2	land8a2	land12a2	land16a2
3	0.561	0.656	0.578	0.518	0.485
5	0.583	0.686	0.633	0.543	0.516
10	0.630	0.750	0.711	0.619	0.581
15	0.658	0.803	0.768	0.696	0.651
20	0.680	0.838	0.810	0.745	0.704
30	0.717	0.883	0.866	0.846	0.774
40	0.739	0.921	0.895	0.877	0.819
50	0.756	0.930	0.907	0.895	0.884
60	0.764	0.937	0.919	0.905	0.896

Table 5.8 Correctness of the dataset

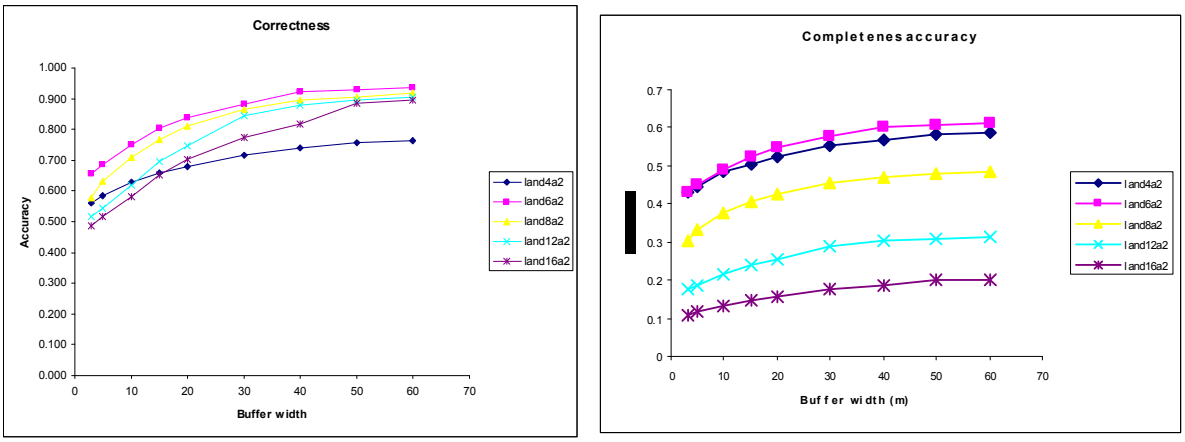

Figure 5.7 left Correctness of dataset and right Completeness of dataset

Buffer	land4a2	land6a2	land8a2	land12a2	land16a2
3	0.322	0.350	0.250	0.153	0.098
5	0.339	0.372	0.280	0.161	0.105
10	0.377	0.421	0.325	0.188	0.120
15	0.401	0.465	0.361	0.217	0.136
20	0.419	0.496	0.388	0.236	0.149
30	0.453	0.537	0.427	0.277	0.166
40	0.473	0.573	0.447	0.290	0.178
50	0.489	0.581	0.456	0.297	0.195
60	0.497	0.589	0.465	0.302	0.198

Table 5.9 Quality of the dataset

For example when extrapolate the graph in figure 5.7 left by assuming that the reference dataset and the extracted dataset approximately are the same, at the minimal buffer (0.0m) the results shows that the correctness of extracted dataset is very low to almost all datasets for having a correctness value bellow 0.5 except for land6a2 which approximately is 0.6 followed by land4a2 which is close to 0.5. By increasing the buffer width the result shows an improvement although in the real sense results into false extraction for linking data close to the reference buffer incorrectly considered as a matched dataset.

Table 5.9 shows the quality of dataset computed using equation 5.3. The results are not clear because of the value obtained from completeness. Completeness indicates the relationship between the extracted data that lies within the buffer around the reference dataset. If the relationship is inconsistence the results proves failure although it doesn't imply for poor extraction as it depend on the reference of data you are using.

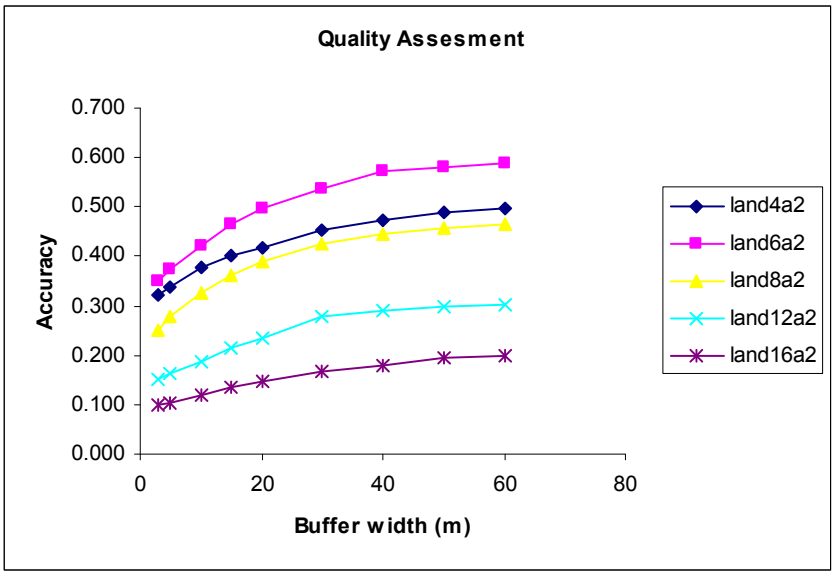

Figure 5.8 percentage quality of dataset

5.5.2. Results based on Visual examination

Three dataset were used test the validity results given in table 5.11, table 5.12 and table 5.13 for land4a2, land6a2 and land8a2 respectively. In the table, the length of the features that were detected by the LSD algorithm and also were identified and measured in the true reference data (geoeye) is compared. The comparison is based on the results obtained from computation of the correctness in percentage that taken as the ratio of the length extracted to the length of true reference. The interpretation of the results is based on the perception judgments of features as indicated in table 5.10

No.	Average Ranges	Interpretation of extracted data
1	less than 45%	poor (few lines were extraction)
2	45% to 64%	Fair (extraction was not normal)
3	65% to 79%	good(the extraction was normal)
4	80% to 100%	Very good (at least all lines was detected)
5	more than 100%	Over detected (possible of false detection)

Table 5.10 Feature interpretations

Land4a2					
Object	**Length Ref**	**Length Extract**	**Integrity**	**percentage matched**	**Interpretation of detection**
FID1	4507.675	4282.910	one to many	0.950	Very good
FID2	308.365	324.076	one to one	1.051	Over extracted
FID3	6808.996	5393.405	many to many	0.792	good
FID4	910.929	847.813	many to many	0.931	Very good
FID5	1872.179	1300.613	one to many	0.695	good
FID6	5951.228	6217.456	one to one	1.045	Over extracted
FID7	10827.934	11293.269	many to many	1.043	Over extracted
FID8	1615.415	1485.474	one to many	0.920	Very good
FID9	3158.886	2699.641	one to many	0.855	Very good
FID10	14705.92	10314.907	many to many	0.701	good
FID11	478.908	396.52	one to many	0.828	good
FID12	1290.807	1196.253	one to many	0.927	Very good
FID13	2551.615	1438.334	many to many	0.564	Fair
FID14	12238.843	12023.176	one to many	0.982	Very good
FID15	3321.165	2260.341	one to many	0.681	good
Average	4703.258	4098.279		0.871	Very good

Table 5.11 Comparison results for land4a2

Land6a2					
Object	**Length Ref**	**Length Extract**	**Integrity**	**percentage matched**	**Interpretation of detection**
FID1	4507.675	4326.307	one to many	0.960	Very good
FID2	308.365	308.126	one to one	0.999	Very good
FID3	6808.996	6191.903	many to many	0.909	Very good
FID4	910.929	483.597	many to many	0.531	Fair
FID5	1872.179	1562.784	one to many	0.835	Very good
FID6	5951.228	5917.243	one to one	0.994	Very good
FID7	10827.934	11275.003	many to many	1.041	Over extracted
FID8	1615.415	1597.165	one to many	0.989	Very good
FID9	3158.886	2985.058	one to many	0.945	Very good
FID10	14705.92	9622.197	many to many	0.654	good
FID11	478.908	441.117	one to many	0.921	Very good
FID12	1290.807	1194.385	one to many	0.925	Very good
FID13	2551.615	1177.049	many to many	0.461	Fair
FID14	12238.843	11923.295	one to many	0.974	Very good
FID15	3321.165	2016.888	one to many	0.607	good
Average	4703.258	4088.141		0.865	Very good

Table 5.12 Comparison results for land6a2

Land8a2					
Object	**Length Ref**	**Length Extract**	**Integrity**	**percentage matched**	**Interpretation of detection**
FID1	4507.675	4226.819	one to many	0.938	Very good
FID2	308.365	257.072	one to one	0.834	Very good
FID3	6808.996	5486.66	many to many	0.806	Very good
FID4	910.929	512.124	many to many	0.562	Fair
FID5	1872.179	1367.698	one to many	0.731	good
FID6	5951.228	5897.983	one to one	0.991	Very good
FID7	10827.934	9951.22	many to many	0.919	Very good
FID8	1615.415	1551.026	one to many	0.960	Very good
FID9	3158.886	2784.24	one to many	0.881	Very good
FID10	14705.92	8738.556	many to many	0.594	Fair
FID11	478.908	369.776	one to many	0.772	good
FID12	1290.807	1278.273	one to many	0.990	Very good
FID13	2551.615	1522.503	many to many	0.597	Fair
FID14	12238.843	11700.04	one to many	0.956	Very good
FID15	3321.165	1168.74	one to many	0.352	Poor
Average	70548.865	56812.730		0.805	Very good

Table 5.13 Comparison results for land8a2

This option gives accuracy in percentage as 87.1, 86.5 and 80.5 for land4a2, land6a2 and land8a2 respectively with an overall percentage of 85.2 when the reference dataset is closely related to the extracted dataset. This result can only interpreted in semantic context as it is difficult to judge on the position accuracy of the extracted dataset by LSD algorithm.

Another observation that can be noticed from table 5.11, table 5.12 and table 5.13 is about the results of individual objects as identified in the origin image compared to that extracted by LSD algorithm. Different results have been observed to different datasets, for example it has been observed that FID4 was well observed in dataset land4a2 compared to the detections observed in land6a2 and land8a2. This may be indicate that feature with low contrast when the implementation involves low threshold value of tolerance angle few lines are detected as the algorithm fail to connect the next point of the same feature that share some qualities. Similar result is very highly observed for FID15 in land8a2 dataset. For curved objects like FID3, FID5 and FID 9 are well identified in land6a2 and land8a2 compared to detections performed in land4a2. The low threshold value still can be applied to curved structure as it is accepted and characterise well the configuration of the object.
For features which are straight and long enough are well detected in both dataset, for visualisation sample datasets are given in figure 5.1 to figure 5.3. In general the detection is not constant depend on the contrast variation of the line segment in that case one line in the reference data can split into multiple in the extracted dataset. The column integrity in table 5.11 to table 5.13 gives general overview of the detection while figure 4.7 in chapter four explain the situation that can happen when determine the length of extracted line segments.

5.6. Summary of the results

Two proposed methods for validating line segment gives convenient results for the performance of LSD algorithm to multispectral images. Using buffer method, the landsat image with spatial resolution of 30m is considered and a buffer width of 15m taken as optimal distance for the extracted line segment. The overall results are given on table 5.12 for land4a2, land6a2 and land8a2.

No.	Quality measure	land4a2	land6a2	land8a2
1	Completeness	0.506	0.525	0.406
2	Correctness	0.658	0.803	0.768
3	Quality	0.401	0.465	0.361

Table 5.14 Summary of quality measure

For this study, the results show that land6a2 gives better results compared to the other datasets. For this case it implies that the addition of parameter *d* at value 6, scale image *s* with value 2 and detection threshold epsilon *e* at 0.0 to LSD algorithm can provide a meaningful extraction of linear feature from multispectral image compared to the default values proposed.

Similarly for visual examination method, the results has been summarized based on object configuration as shown in table 5.15, the overall assessment of the results still shows land6a2 gives the better results for the sample datasets used in the validation.

No.	FID Involved	Feature Description	Percentage average value		
			land4a2	land6a2	land8a2
1	1, 2, 4, 6, 7, 10, 14	Straight and long enough	0.950	0.879	0.828
2	3, 11	Normal curved feature	0.810	0.915	0.789
3	9, 8, 12	Complex curved feature	0.901	0.953	0.944
4	5, 13, 15	Narrow path feature	0.647	0.634	0.560
5	Overall assessment		0.827	0.845	0.780

Table 5.15 Summary for visual interpretation

6. General discussion

6.1. Introduction

This chapter discusses the general overview on LSD algorithm used in this study to extract meaningful line segments from multispectral remotely sensed data. Different parameters used by the algorithm are discussed. Their performance and limitations are discussed as well based on experiments performed in this study.

6.2. Performance of LSD algorithm

LSD algorithm includes three parameters in search of maximal meaningful line segment from multispectral image. Table 5.1 of chapter 5 illustrates the parameters used in this study. The performance and limitation of each parameter is discussed in the following sections of this chapter.

6.2.1. The effect of parameter (d)

In this research a line segment refers to a straight feature that connect group of points that share the same gradient angle to a certain tolerance. Parameter d is a number of gradient orientations and is an important element in those algorithms that use the gradient orientation to group pixels into line support region. This parameter in [44] has been described in details where by the 2π radiant range of gradient orientation is converted into 8 equal interval each of which is $\pi/4$ as illustrated in figure 6.1 left. Grouping of these pixels into line support region vary with the number of orientations as described in figure 6.1 right when the number of orientation is 8.

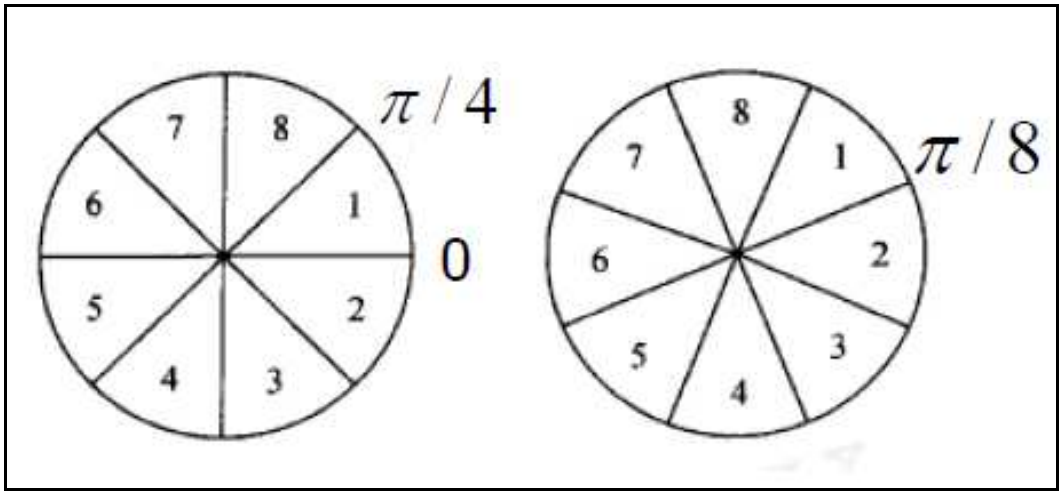

Figure 6.1 Gradient orientation partitioning

The effect of parameter d has been observed at a low threshold value where many gaps were detected as shown in figure 5.2 of chapter 5. Many gaps was observed in figure 5.3. This implies that when the image partitioned into line support region the algorithm in search of connecting groups of points that

share the same gradient angle fail to connect the next point because these points either belong to another region or have low intensity contrast. The algorithm stops detecting homogeneous pixels thereby and introduces the gaps. At high threshold value the algorithm may include adjacent points that share the same gradient angle in the same radiant interval as illustrated in figure 6.1. This can be observed in areas enclosed with blue lines in figure 5.1-5.3 where many gaps and few lines are detected at low threshold and vice versa.

Another effect was observed on different shapes available patterns in an image. Oval shaped patterns are optimally detected when the number of gradient orientation is large. Linear features with irregular shapes are generalized when the number of gradient orientation is small resulting into false detection. These shapes can be observed in figure 5.1-5.3 enclosed with red lines.

Parameter *d*, when properly selected, can perform better in high and medium resolution images as observed in this study. However, the parameter may not perform well in coarse resolution images where the pixel is more uncertain due to mixed land cover classes.

Detailed information on parameter d can be studied by the graphs in figure 5.4 on which figure 5.4 left shows the average total number of extracted line segment with respect to the change in parameter d . The graph shows the positively skewed number of detected line segments when the value of *d* is increased. The problem of this parameter lies on how to arrive at a right value for optimal line segments detection.

6.2.2. The effect of parameter s

Parameter s is the smoothing parameter often used to emphasize a certain feature by controlling the pixel intensity contrast. The object information in the image can be perceived at certain scale and only if the noisy in the image is removed otherwise may render to the useless result. Table 5.4 is the summary of the results at different scale. For visualization of the trend due to change of scale can be studied from graph in figure 5.5.

In LSD algorithm parameter *s* helps to control the false detection due to the presence of noisy in the image. In this study the results show that when scale increases more line segments are detected at a certain fixed value of gradient orientation as illustrated in table 5.4. In addition, the results show that the parameter is affected by the change of the number of gradient orientation. For example, table 5.4 when *s* is 2.0 and d is 4, 3057 number of lines were detected and when d is 16, 1137 number of lines were detected with the same value of scale. These detection results give 1920 different number of lines. The large difference shows how parameter *d* is very sensitive to LSD algorithm.

6.2.3. The effect of parameter e

Parameter e is the detection threshold epsilon expressed as a measure of maximum number of false detection. At a minimal value of *e* the algorithm detects finer lines. Table 5.6 of chapter 5 shows that parameter e is not a critical one as the results are less dependent on it. For example the range between 0 and 0.1 it is difficult to detect the changes in the number detected lines by the algorithm. By changing values for this parameter results into a decrease in number of detected lines indicating that the precision within the dataset has decreased as indicated in table 5.6.

Another observation on this parameter is on the rate of change of the number of lines detected within at a certain threshold value. For example, the rate of change of lines detected with parameter d when is 4 and parameter d when is 16 at detection threshold value 0.0 and 80, the graph of figure 5.6 left shows that the greater the number of gradient orientation the more rapid the number of lines decreases with respect to the increase of the threshold detection value. But when smaller number of gradient orientation is used the rate of change of the number of line segments detected decreases.

6.3. Other comparison methods

Feature extraction involves simplifying the amount of resources required from the digital images to describe a large set of data accurately that can help in object recognition. In extraction of line segment four categories that classifies the line segment model used in different literature includes Statistical based, Gradient orientation based, Pixel connectivity edge linking based and Hough transform [44]. In this part of discussion each method will be considered in brief by looking on the limitations compared to LSD algorithm.

6.3.1. Gradient orientation base

Gradient orientation based uses an algorithm which partitioned an image into line support regions of equal interval [44]. In this method each pixels in the gradient orientation belongs to one interval and it is labelled according to the partitioning in which it falls. This method is also called Burns et al. method. The limitation of this method is the presence of noise in the detected image as the method performed without a false detection control. Although the detection is performed but it is a useless result as it is difficult to identify an object boundary in the noise image [28]. This limitation has been improved in LSD algorithm as it uses the false detection control to avoid the noise in the resulting image.

6.3.2. Hough Transform

Hough Transform, also known as Standard Hough Transform (SHT), is a global method based on accumulator cells which record all possible sought shapes passing through each extracted edge point [45]. This method shows several errors including the influence of isolated pixels as well as the computing time requirements being among the biggest noticeable problems. Despite the fact that the SHT carry on noise and discontinuity in image, it has some inherent limitations such as high computing time, unmanageable memory requirement, low peaks for short lines and incapability in preserving edge pixel connectivity. This limitation has restricted the usage of Hough transform to only image of small size [28]. When compared to LSD algorithm these limitations have been improved or removed completely in LSD algorithm. LSD algorithm is linear time detector and also gives accurate detection and control number of detection. LSD only does not detect any structure in the noise image although does not produce false detection.

Other comparison need further findings but through the limitations mentioned above LSD algorithm gives accurate results and controlled number of false detections compared to the other methods of line segment detection.

7. Conclusion and Recommendation

7.1. Conclusion

The overall objective of this research is to add the new method in remote sensing image analysis by adapting one of existing algorithm based on Gestalt theory of visual perception in extraction of information from multispectral image. To achieve this objective three relevant questions corresponding to sub objectives were posed and have to be answered.

The first question is how do algorithm based on Gestalt principle applied to remotely sensed images? In this study, implementation of algorithm based on Helmholtz principle was applied in extraction of linear feature in the remotely sensed image. Helmholtz principle is a perceptual principle that uses statistical model based on a contrario approach for detection of linear feature in the non structures data. In this case the algorithm uses the false detection control in order to obtain a clear structure from random noise image. The results obtained by applying these algorithm its geometric structures was analysed and the assessment of the quality of the results were able to be performed.

The second question is how can Gestalt grouping laws be applied in feature detection from remotely sensed image? This question involves a region growing subprogram that has been included in LSD algorithm. In this study the grouping laws gave an insight on how pixels are combined together when they constitute the common characteristics. The region growing algorithm applied by select a seed point with high intensity contrast and then the seed point start connecting other point based on their similarity and their tolerance level line angle which was set form the number of gradient orientation. Taking into account the similarity of object and connecting the feature in a good continuous form the line segment were observed.

The third question is how can the best threshold values of parameters be found that an involved algorithm based on the Gestalt principle for feature detection applied to remotely sensed images? Linear detection from remotely sensed images aim at finding sharp changes in image brightness so as to capture important events and changes in properties boundaries that correspond to discontinuities in surface orientation. In finding best parameter values based on different experiments the best values to the parameter involved that gave meaningful and optimal results was identified. LSD algorithm is the parameterless that were tested to different grey level images and obtained better results. On my findings it has been observed that this algorithm can only perform well to multispectral images when the parameters are tuned to some threshold values. Three parameters which are Tolerance of the level line angle, image scale and the detection threshold epsilon was tested and evaluated.

Based on the evaluation of the results of extracted linear feature by LSD algorithm the following conclusion can be drawn

- Application of an algorithm based on Gestalt principles to remotely sensed images performed well for general image analysis although the performance can be improved by varying the

respective parameters, three parameters has been involved; tolerance of level line angle, image scale and detection threshold epsilon

- The tolerance angle shows the greater effect to the result such that at low threshold value the detection is minimum compared with detection at large value. The proposed optimal range for parameter is 22.5 to 60 degrees which is equivalent when the number of orientation is 8 and 3 respectively, figure 4.5 in chapter four illustrates.
- Also the performance of an algorithm when considering the image scale parameter the results shows that at maximum threshold value of 2 more detection are found. This has been illustrated in figure 4.5 where the number of line segment and the total length of line segment are obtained when the threshold value is 2.Similarly the detection threshold epsilon e the maximum detection value occurs when the parameter value is 0.0.

Combining these parameters with optimal threshold values, the evaluation shows that the dataset obtained with tolerance angle at 30^{o}, image scale of 2 and detection threshold of 0.0 gives the better results when the multispectral image applied, for example the landsat ETM+ that used in this study. Improvement can be done on the value of tolerance of the level line angle as in this study shows to be very sensitive in varying the results.

From these results, I can conclude that the proposed LSD algorithm is a robust algorithm as it gives accurate results for multispectral images when the parameter is tuned. The algorithm is easier to use for general image analysis when the implementation is done in Megawave2 software, several editing can be performed for the purpose of improving the linear detection results.

7.2. Recommendation

This research shows the possibility of obtaining better results in the implementation of gestalt principles for linear feature detections using remotely sensed data. The absence or presence of gaps in different results of the dataset tested in this research is an indication of causes of an error in the position, size, orientation and even threshold settings for respective feature to be detected. Therefore these drawbacks require more investigation to improve the detection results. For further improvement of this results I do recommend as the following

- Proper method of band selection that maximizes the interested information must be taken into consideration. This is because the algorithm uses intensity contrast value of the pixel in search of the presence or not of line segment. This can either be done by involving different bands and visualise the results by comparing with the original image as a preliminary study.
- More investigation on other possible parameters can be done to improve the results for extraction for further research, for example the implementation of law of closure as proposed in Gestalt principle of perceptual organization computer can be trained to reduce these gaps that appear in the resulting datasets
- Another recommendation is on the improvement of validation methods based on visual examination method as it performed manually due to lack of proper reference dataset to be used. This method requires prior knowledge for the area of interest and the proper study on creating standard values for visual interpretation of extracted data compared to the reference data.

References

1. Yan, G., *Pixel based and object oriented image analysis for coal fire research*. 2003, ITC: Enschede. p. 82.
2. Campbell, J.B., *Introduction to remote sensing*. 4th. ed. ed. 2007, New York: Guilford. 626
3. Lillesand, T.M., R.W. Kiefer, and J.W. Chipman, *Remote sensing and image interpretation*. 6th ed. ed. 2008, New York: Wiley. p.756-768.
4. Bemigisha, J., *Spectral and human sensors: hyperspectral remote sensing and participatory GIS for mapping livestock grazing intensity and vegetation in transhumant Mediterranean conservation areas*. ITC publication; no. 155. 2008. p.156-172.
5. Kerle, N., L.L.F. Janssen, and W.H. Bakker, *Principles of remote sensing: An introductory textbook*. 3rd. ed. ITC educational textbook series, 2. 2004, Enschede: ITC. p.250.
6. Townshend, J., *Review: Computer processing of remotely sensed images, an introduction* The Geographical Journal, 1988. **154**(2): p. 297.
7. Rosenfeld, A., *Image analysis and computer vision: 1990.* CVGIP: Image Understanding, 1991. **53**(3): p. 322-365.
8. Stein, A., *Handling uncertainties in image mining for remote sensing studies.* In: Proceedings of the 8th international symposium on spatial accuracy assessment in natural resources and environmental sciences, Shanghai, P.R. China, June 25-27, 2008 Liverpool: M.F. World Academic Press, 2008. 170-1 pp. 362-368, 2008.
9. Desolneux, A. and L. Moisan. *From Gestalt Theory to Image Analysis A Probabilistic Approach* 2007; Available from: http://www.math-info.univ-paris5.fr/map5/publis/PUBLIS06/2006-9.pdf.
10. Stein, A., *Modern developments in image mining.* In: Science in China series E : technological sciences, 51(2008) supp. 1. pp. 13-25, 2008.
11. Bertels, L., *Hyperspectral remote sensing of vegetation in the dynamic dunes along the Belgian coast*. 2005, Heerlen: Open Universiteit Nederland. 101.
12. Richards, J.A. and X. Jia, *Remote sensing digital image analysis: An introduction*. Fourth edition ed. 2006, Berlin Springer-Verlag. p.439.
13. Weber, M., *Empiricism, gestalt qualities, and determination of style: Some remarks concerning the relationship of Guido Adler to Richard Wallaschek, Alexius Meinong, Christian von Ehrenfels, and Robert Lach*. 1997. p. 42-56.
14. Kurt, K. and W. Max. *Psychologische Forschung (Springer-Verlag.) http://www.getcited.org/pub/100004322*. 2008; Available from: http://www.getcited.org/pub/100004322.
15. Simon, D. and K.J. Holyoak, *Structural dynamics of cognition: From consistency theories to constraint satisfaction.* Personality and Social Psychology Review, 2002. **6**(4): p. 283-294.
16. Green, C.D. *Classics in the History of Psychology -- Glossary to Koffka (1922) by C.D. Green*. 2002; Available from: http://www.psych.yorku.ca/classics/Koffka/Perception/glossary.htm.
17. Breidbach, O. and J. Jost, *On the gestalt concept.* Theory in Biosciences, 2006. **125**(1): p. 19-36.
18. Desolneux, A., L. Moisan, and J.-M. Morel, *Computational gestalts and perception thresholds.* Journal of Physiology-Paris, 2003. **97**(2-3): p. 311-324.
19. Baker, J., D.R. Jones, and J. Burkman, *Using Visual Representations of Data to Enhance Sensemaking in Data Exploration Tasks.* Journal of the Association for Information Systems, 2009. **10**(7): p. 533-559.
20. Desolneux, A., L. Moisan, and J.M. Morel, *Maximal meaningful events and applications to image analysis.* Annals of Statistics, 2003. **31**(6): p. 1822-1851.

21. Desolneux, A., L. Moisan, and J.M. Morel, *A grouping principle and four applications.* Ieee Transactions on Pattern Analysis and Machine Intelligence, 2003. **25**(4): p. 508-513.
22. Carsetti, A., *The Embodied Meaning: Self-Organisation and Symbolic Dynamics in Visual Cognition*. 2004. p. 307-330.
23. Desolneux, A., L. Moisan, and J.-M. Morel, *Computational gestalts and perception thresholds.* Journal of Physiology-Paris. **97**(2-3): p. 311-324.
24. Coupier, D., A. Desolneux, and B. Ycart, *Image Denoising by Statistical Area Thresholding.* Journal of Mathematical Imaging and Vision, 2005. **22**(2): p. 183-197.
25. Cantú-Paz, E., *Parameter Setting in Parallel Genetic Algorithms*. 2007. p. 259-276.
26. Jackson, Q. and D.A. Landgrebe, *Adaptive Bayesian contextual classification based on Markov random fields.* Ieee Transactions on Geoscience and Remote Sensing, 2002. **40**(11): p. 2454-2463.
27. Froment J, *Megawave user guide.* The Preliminary Guides to the Megawave Software, version 3.01, 2007. **1**: p. 4-5.
28. Grompone von Gioi R., M. J. Morel, G. Randall, J. Jakubowicz *LSD: A Fast Line Segment Detector with a False Detection Control.* . 2008 [cited 2009 February 08]; Available from: http://mw.cmla.ens-cachan.fr/megawave/algo/lsd/.
29. Zhan, Q., M. Molenaar, K. Tempfli and W.Z.Shi, *Quality assessment for geo - spatial objects derived from remotely sensed data.* International journal of remote sensing, 2005. **26**(14).
30. Dutton, W.H., *Information and communication technologies: visions and realities*. 1996, Oxford etc.: Oxford University Press. p.464.
31. Shi, W.Z., *Modelling positional and thematic uncertainties in integration of remote sensing and geographic information systems*, in *ITC Dissertation;14*. 1994, ITC: Enschede. p. 147.
32. Goodchild, M.F.e. and S. Gopaleditor, *accuracy of spatial databases*. 1989, London etc.: Taylor & Francis. p.290.
33. Hunter, G.e. and K.e. Lowell, *Accuracy 2002 : proceedings of the 5th international symposium on spatial accuracy assessment in natural resources and environmental sciences, Melbourne, Australia, July 10 - 12*. 2002, Delft: Delft University Press. 546.
34. Heipke C, Mayer H, and Wiedemann C, *Evaluation of automatic road extraction.* Chair for Photogrammetry and Remote Sensing, 1997(Technische Universit ¨at M¨unchen, D–80290 Munich, Germany).
35. Leclerc, Y.G., *Simplicity of Description: as a basis for visual interpretation.* International Journal of Computer Vision, 1989. **Volume 3**: p. 73-102.
36. Mitiche, A. and S. Hadjres, *MDL estimation of a dense map of relative depth and 3D motion from a temporal sequence of images.* Pattern Analysis and Applications, 2003. **6**(1): p. 78-87.
37. Tversky, T., W.S. Geisler, and J.S. Perry, *Contour grouping: closure effects are explained by good continuation and proximity.* Vision Research, 2004. **44**(24): p. 2769-2777.
38. Coster, M. and J.-L. Chermant, *Image analysis and mathematical morphology for civil engineering materials.* Cement and Concrete Composites. **23**(2-3): p. 133-151.
39. Kraak, M.J. and F.J. Ormeling, *Cartography : visualization of geospatial data*. Second edition ed. Also available in Indonesian : Kartografie visualisasi data geospasial. 2003, Harlow: Addison Wesley, Longman. 205.
40. Moore, P.A., *Topographic maps in US libraries.* International Library Review, 1987. **19**(3): p. 201-223.
41. Andrews, J.H., *The history of topographical maps: Symbols, pictures and surveys: P. D. A. Harvey,.* Journal of Historical Geography, 1982. **8**(2): p. 219-220.
42. Thunnissen, H. and A. De Wit. *The national land cover database of the Netherlands*. 1999: ISPRS, Amsterdam, 2000.
43. Gioi, von, R.G., M. J. Morel, G. Randall, J. Jakubowicz, *On straight line segment detection.* Journal of Mathematical Imaging and Vision, 2008. **32**(3): p. 313-347.
44. Guru, D., B. Shekar, and P. Nagabhushan, *A simple and robust line detection algorithm based on small eigenvalue analysis.* Pattern Recognition Letters, 2004. **25**(1): p. 1-13.

45. Duda, R. and P. Hart, *Use of the Hough transformation to detect lines and curves in pictures.* 1972.

Appendices

Appendix A: georeferencing result

Table A.1 Transformation accuracy for Landsat Image

Row	Point ID	X Input	Y Input	X Ref.	Y Ref.	X Residual	Y Residual
1	GCP #2	39.967	-112.232	174347.656	517777.346	-0.002	-0.003
2	GCP #4	289.430	-375.026	181803.460	509913.458	0.014	0.016
3	GCP #5	15.706	-204.352	173612.164	515007.287	0.018	0.008
4	GCP #6	155.172	-207.172	177793.615	514939.435	0.016	0.006
5	GCP #7	161.248	-86.534	177986.005	518563.941	-0.022	-0.007
6	GCP #8	211.466	-389.489	179463.701	509468.401	-0.009	-0.021
7	GCP #9	86.502	-464.343	175709.553	507205.132	-0.014	0.001

Overall RMS Error in y= 0.01111
Overall RMS Error in x= 0.0148
Overall RMS Error = 0.0185

Table A.2 Transformation accuracy for Geoeye Image

Row	Point ID	XInput	YInput	X Ref.	Y Ref.	X Res	Y Res
1	GCP #2	584.178	-407.048	174347.657	517777.339	-0.004	0.012
2	GCP #4	2794.916	-2774.978	181803.460	509913.452	-0.004	-0.007
3	GCP #5	364.501	-1233.496	173612.164	515007.280	0.002	-0.014
4	GCP #6	1606.305	-1263.304	177793.615	514939.428	-0.004	0.009
5	GCP #7	1665.056	-180.131	177986.006	518563.934	0.005	-0.007
6	GCP #8	2099.834	-2902.733	179463.701	509468.394	0.005	0.007

Overall RMS Error in X = 0.0043
Overall RMS Error in Y = 0.0096
Overall RMS Error = 0.0106

Appendix B: Vector transformation results

Table B.1 adjustment accuracy for Land4a2

Point ID	X-source	Y-source	X-destination	Y-destination	RMS Error
1	290.459	-375.546	181803.460	509913.458	0.376
2	12.721	-202.832	173612.164	515007.287	0.182
3	147.846	-216.146	177793.615	514939.435	0.141
4	144.451	-110.022	177986.005	518563.941	0.541
5	215.408	-381.732	179463.701	509468.401	0.437

Overall RMS Error = 0.2863

Table B.2 Adjustment accuracy for Land6a2

Point ID	X-source	Y-source	X-destination	Y-destination	RMS Error
1	60.506	-376.492	175285.455	509334.569	0.383
2	40.978	-112.071	174331.641	517858.992	0.284
3	350.989	-112.922	183106.030	518612.544	0.285
4	289.804	-375.991	181804.417	509913.574	0.384

Overall RMS Error = 0.3378

Table B.3 Adjustment accuracy for Land8a2

Point ID	X-source	Y-source	X-destination	Y-destination	RMS Error
1	22.012	-26.913	173688.884	520612.436	0.690
2	351.023	-113.000	183105.976	518611.849	0.412
3	289.774	-374.906	181804.326	509912.912	0.592
4	60.457	-376.501	175285.362	509333.989	0.426
5	40.899	-122.154	174332.111	517859.001	0.63

Overall RMS Error = 0.5629

Appendix C: Statistical results of computations of line segments

Table C.1 Total number of line segments

Total number of line segments						
code ID	d=16	d=12	d=8	d=6	d=4	sum
a	1137	1767	2551	2921	3057	11433
b	1205	1678	2186	2367	2344	9780
c	704	912	1069	1066	897	4648
e	1133	1762	2535	2908	3041	11379
f	1193	1663	2169	2354	2329	9708
g	687	906	1048	1038	885	4564
i	1135	1767	2543	2921	3049	11415
j	1205	1678	2186	2367	2344	9780
k	691	912	1058	1065	896	4622
m	1137	1767	2545	2921	3057	11427
n	1205	1678	2186	2367	2344	9780
p	704	912	1069	1066	897	4648
sum	12136	17402	23145	25361	25140	
Average	1011.333	1450.167	1928.75	2113.417	2095	

Table C.2 The total length of line segment

Total length of line segment						
code ID	d=16	d=12	d=8	d=6	d=4	sum
a	11765	17910	27567	34067	40902	132211
b	13686	19502	27575	32695	37736	131194
c	11376	15209	20063	22745	24272	93665
e	11735	17889	27495	33988	40808	131915
f	13629	19417	27465	32603	37628	130742
g	11227	15142	19878	22434	24126	92807
i	11750	17910	27532	34067	40858	132117
j	13686	19502	27575	32695	37736	131194
k	11264	15208	19963	22736	24263	93434
m	11765	17910	27544	34067	40902	132188
n	13686	19502	27575	32695	37736	131194
p	11376	15209	20063	22745	24272	93665
sum	146945	210310	300295	357537	411239	
Average	12245.42	17525.83	25024.58	29794.75	34269.92	

Appendix D: Computed total reference of line segment and total length of extracted line segment

Table D.1 Total length (TL) of lines extracted for Land4a2

Buffer	TL Ref	TL Extract	TP	FN	FP
3	1563944	1201647	674106	889838	527541
5	1563944	1201647	700459	863485	501188
10	1563944	1201647	756801	807143	444846
15	1563944	1201647	790963	772981	410684
20	1563944	1201647	816621	747323	385026
30	1563944	1201647	861969	701975	339678
40	1563944	1201647	888220	675724	313427
50	1563944	1201647	908081	655863	293566
60	1563944	1201647	918411	645533	283236

Table D.2 Total length (TL) of lines extracted forLand6a2

Buffer	TL Ref	TL Extract	TP	FN	FP
3	1563944	1022546	670446.9	893497.1	352099.1
5	1563944	1022546	701803.7	862140.3	320742.3
10	1563944	1022546	766932.6	797011.4	255613.4
15	1563944	1022546	821365.8	742578.2	201180.2
20	1563944	1022546	857149.9	706794.1	165396.1
30	1563944	1022546	903259.5	660684.5	119286.5
40	1563944	1022546	941693.5	622250.5	80852.52
50	1563944	1022546	950626.6	613317.4	71919.35
60	1563944	1022546	958312.8	605631.2	64233.18

Table D.3 Total length (TL) of lines extracted forLand8a2

Buffer	TL Ref	TL Extract	TP	FN	FP
3	1563944	825564.1	477231	1086713	348333.1
5	1563944	825564.1	522898.4	1041046	302665.8
10	1563944	825564.1	586719.6	977224.4	238844.5
15	1563944	825564.1	634208.3	929735.7	191355.8
20	1563944	825564.1	668317.4	895626.6	157246.7
30	1563944	825564.1	715255.4	848688.6	110308.8
40	1563944	825564.1	738615	825329	86949.15
50	1563944	825564.1	748855.5	815088.5	76708.63
60	1563944	825564.1	758916.8	805027.2	66647.37

Table D.4 Total length (TL) of lines extracted forLand12a2

Buffer	TL Ref	TL Extract	TP	FN	FP
3	1563944	538204	278963.7	1284980	259240.3
5	1563944	538204	292092	1271852	246112
10	1563944	538204	333104.8	1230839	205099.2
15	1563944	538204	374400	1189544	163804
20	1563944	538204	401024	1162920	137180
30	1563944	538204	455401.4	1108543	82802.56
40	1563944	538204	471987	1091957	66216.98
50	1563944	538204	481519.6	1082424	56684.36
60	1563944	538204	487009.1	1076935	51194.94

Table D.5 Total length (TL) of lines extracted forLand16a2

Buffer	TL Ref	TL Extract	TP	FN	FP
3	1563944	353055	171387	1392557	181668
5	1563944	353055	182139	1381805	170916
10	1563944	353055	205075	1358869	147980
15	1563944	353055	229750	1334194	123305
20	1563944	353055	248614	1315330	104441
30	1563944	353055	273259	1290685	79796
40	1563944	353055	289132	1274812	63923
50	1563944	353055	312265	1251679	40790
60	1563944	353055	316187	1247757	36868